Proton and Ion Linear Accelerators

Yuri Batygin[1], Sergey Kurennoy[1], Sebastian Szustkowski[1], Salvador Sosa Guitron[1], Vyacheslav Yakovlev [2],

[1]Los Alamos National Laboratory

[2]Fermi National Accelerator Laboratory

U.S. Particle Accelerator School

July 15 – July 26, 2024

Proton and Ion Linear Accelerators

Periodic structures, Standing-wave cavites, Lecture 12

Vyacheslav Yakovlev, Fermilab

U.S. Particle Accelerator School (USPAS)

Education in Beam Physics and Accelerator Technology

July 23, 2024

RF accelerating structures

Outline:

4. Periodic acceleration structures;
5. Standing –Wave acceleration structures;
6. Why SRF cavities?

Chapter 4.

Periodic acceleration structures.

a. Coupled cavities and periodic structure;
b. Travelling waves in a periodic structure;
c. Dispersion curve;
d. Phase and group velocities;
e. Parameters of the TW structures;
f. Equivalent circuit for a travelling – wave structure;
g. Losses in the TW structure;
h. Types of the TW structures;
i. Examples of modern TW structures.

Periodic acceleration structures:

- Single – cell cavities are not convenient to achieve high acceleration: a lot of couplers, tuners, etc.
- Especially it is important for electron acceleration:

  $R_{sh} = R/Q \cdot Q_0 \sim \omega^{1/2}$, low Ohmic losses at high frequency;

  $v=c$, focusing is quadratic and does not depend on frequency.

high frequencies are preferable (typically up to few tens of GHz).

small cavity size, ~ 1 cm for RT, ~20 cm for SRF

periodic structure of coupled cells.

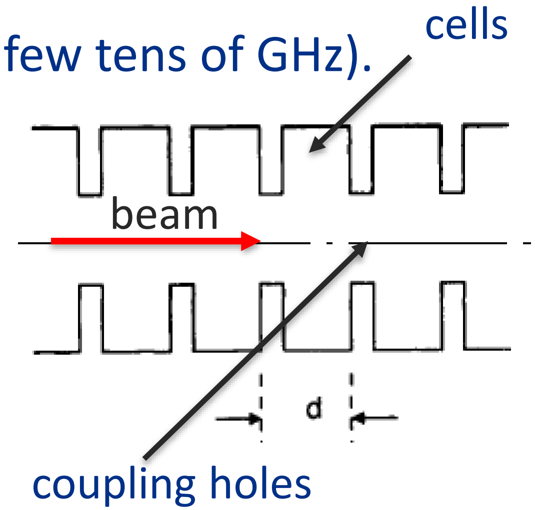

- To provide synchronism with the accelerated particle, the particle velocity $v_p=\beta c=v_{ph}=\omega/k_z$ and the structure period $d = \varphi/k_z = \varphi\lambda/(2\pi\beta)$; φ is phase advance per period, $\varphi = k_z d$.

Periodic acceleration structures:

- Each previous cell excites EM filed in a current cell, which in turn excites the field in the next cell.

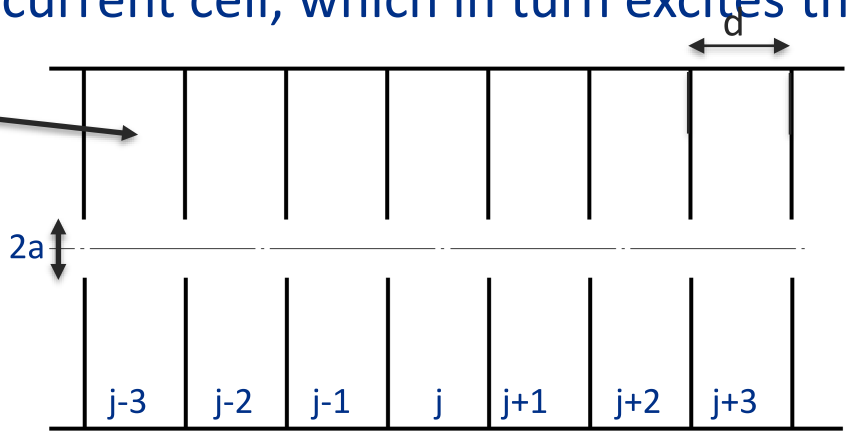

- Cavity excitation by surface tangential electric field:

  $\vec{E}_j = \sum_{i=0}^{\infty} X_{ij}\vec{E}_i$ - field in the j[th] cell;

  $\vec{E}_i$ - eigen functions of cells.

- Single-mode approximation:

  $\vec{E}_j = X_j\,\vec{E}_0$ - field in the j[th] cell . Works everywhere except the hole

  $\vec{E}_0$ - eigen function of the operation TM_{010} mode of a cell.

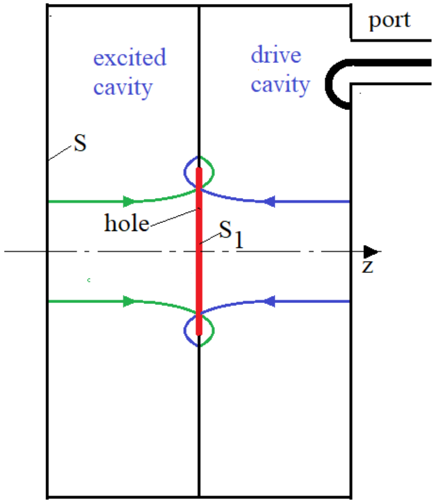

- Excitation of a cavity by the field of a similar neighboring cavity through a small hole:
- Boundary conditions for the excited cavity field $\vec{\boldsymbol{E}}$: $E_t = 0$ on S; $E_t = \vec{\mathbf{E}}_t$ on S_1 (hole). For eigenfunction $E_{0t} = 0$ on S+ S_1
- From Maxwell equations for eigenfunction and excited field:

$$X = \frac{\int_{S_1} \vec{\mathbf{E}}\times\vec{H}_0 dS}{2\omega W\left(1-\frac{\omega_0^2}{\omega^2}\right)},$$

here $\vec{H}_0$ is eigen magnetic field, W -stored energy ω_0- eigen frequency, ω- drive frequency.

(Exact derivation is in the Appendix 11)

Amplitude X is the same as for a parallel oscillator

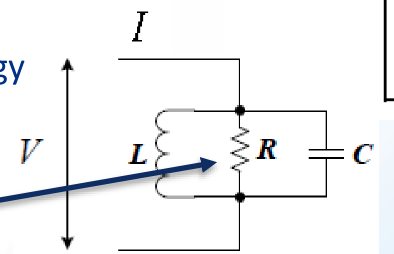

Fermilab

Periodic acceleration structures:

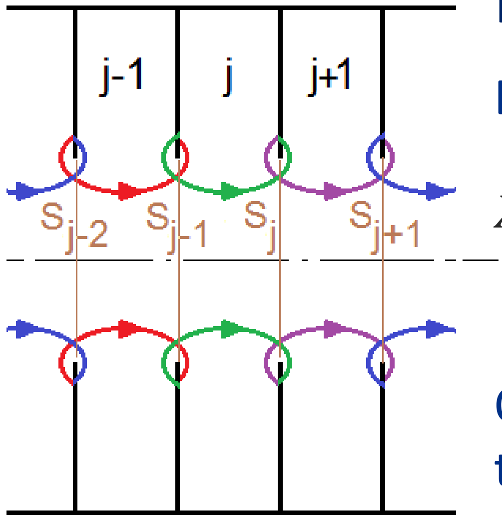

In the j[th] cell $\vec{E}_j = X_j \vec{E}_0$

Excitation of a cavity by surface electric field:

$$X_j = \frac{\int_{S_{j-1}} \vec{E}_{j-1} \times \vec{H}_0 dS}{2\omega W\left(1-\frac{\omega_0^2}{\omega^2}\right)} + \frac{\int_{S_j} \vec{E}_j \times \vec{H}_0 dS}{2\omega W\left(1-\frac{\omega_0^2}{\omega^2}\right)} \qquad (1)$$

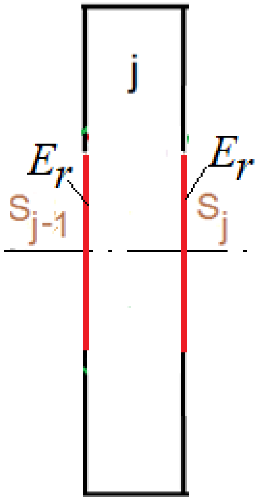

On the coupling holes tangential electric is superposition of the fields of the current cell and the neighboring cell:

$$\int_{S_{j-1}} \vec{E}_{j-1} \times \vec{H}_0 \, dS = K\omega_0 W\left(X_j - X_{j-1}\right), \qquad \int_{S_j} \vec{E}_j \times \vec{H}_0 \, dS = K\omega_0 W\left(X_j - X_{j+1}\right), \ (2)$$

here $K = \frac{1}{W\omega_0} \int_S \vec{\mathrm{E}}_0 \times \vec{H}_0 \, dS$- dimensionless constant depending on the cavity shape.

Therefore, from (1) and (2) one has:

$$X_j\left(1 - \frac{\omega_0^2}{\omega^2}\right) - \left(K\frac{\omega_0^2}{\omega^2}X_j - \frac{1}{2}K\frac{\omega_0^2}{\omega^2}X_{j-1} - \frac{1}{2}K\frac{\omega_0^2}{\omega^2}X_{j+1}\right) = 0,$$

or

$$X_j\left(1 - (1+K)\frac{\omega_0^2}{\omega^2}\right) + \frac{1}{2}K\frac{\omega_0^2}{\omega^2}\left(X_{j-1} + X_{j+1}\right) = 0 \qquad (1)$$

(Exact derivation is in the Appendix 11)

Periodic acceleration structures:

- For a pillbox K depends on the aperture as a^3:
- In paraxial approximation E_{z0} for TM$_{010}$ modes in a pillbox cavity does not depend on r in cylindrical coordinates $\vec{r}, \vec{\varphi}, \vec{z}$, see Lecture 1, slide 49.
- In presence of a small hole radial electric field $E_{r0} \sim r$ next to the hole.
- On the other hand, $div\vec{E} = \frac{1}{r}\frac{\partial(rE_r)}{\partial r} + \frac{\partial E_z}{\partial z} = 0 \rightarrow E_{r0}(r) = -\frac{r}{2}\frac{\partial E_z}{\partial z} \approx \frac{rE_{z0}}{4a}$;

$$H_{\varphi 0}(r) = \frac{1}{2i\omega a}\int_0^r E_{z0} r dr \sim r, \text{ and } \int_{S_{j-1}} E_{r0} H_{\varphi 0} dS \sim a^3$$

- For pillbox cells having thin walls and a hole with the radius a one has

$$K = \frac{2E_0^2 a^3}{3Z_0 W_0 c} = \frac{2}{3} \cdot \frac{R/Q}{Z_0} \cdot \frac{k_0 a^3}{d^2 T^2} \qquad k_0 = \frac{\omega_0}{c}$$

(Exact derivation is in the Appendix 11)

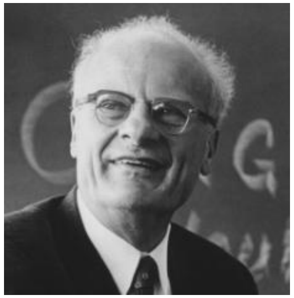

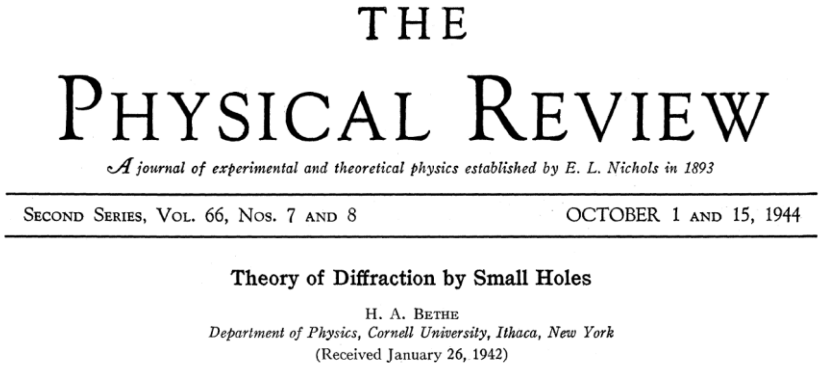
THE

PHYSICAL REVIEW

A journal of experimental and theoretical physics established by E. L. Nichols in 1893

SECOND SERIES, VOL. 66, NOS. 7 AND 8 OCTOBER 1 AND 15, 1944

Theory of Diffraction by Small Holes

H. A. BETHE

Department of Physics, Cornell University, Ithaca, New York

(Received January 26, 1942)

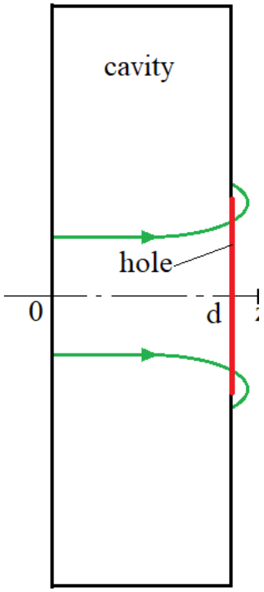

Pillbox cavity with a hole

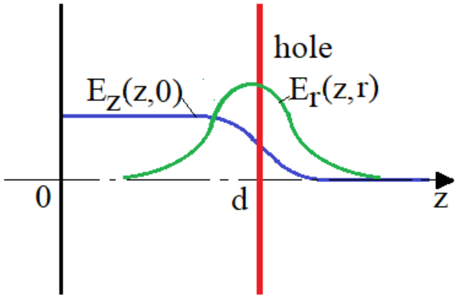

Axial and radial filed distribution along the Axis. Scales for E_z and E_r are different.

Travelling–Wave acceleration structures:

In the infinite chain of cavities equation $X_j\left(1-(1+K)\frac{\omega_0^2}{\omega^2}\right)+\frac{1}{2}K\frac{\omega_0^2}{\omega^2}\left(X_{j-1}+X_{j+1}\right)=0$ (1) has solution (travelling wave):

$X_j = Xe^{ij\varphi}$ (2)

- From (1) and (2) it follows

$$1 = (1+K)\frac{\omega_0^2}{\omega^2}+\frac{1}{2}K\frac{\omega_0^2}{\omega^2}\left(e^{i\varphi}+e^{-i\varphi}\right)$$

or

$$\omega(\varphi) = \omega_0[1+K(1-cos\varphi)]^{1/2}$$

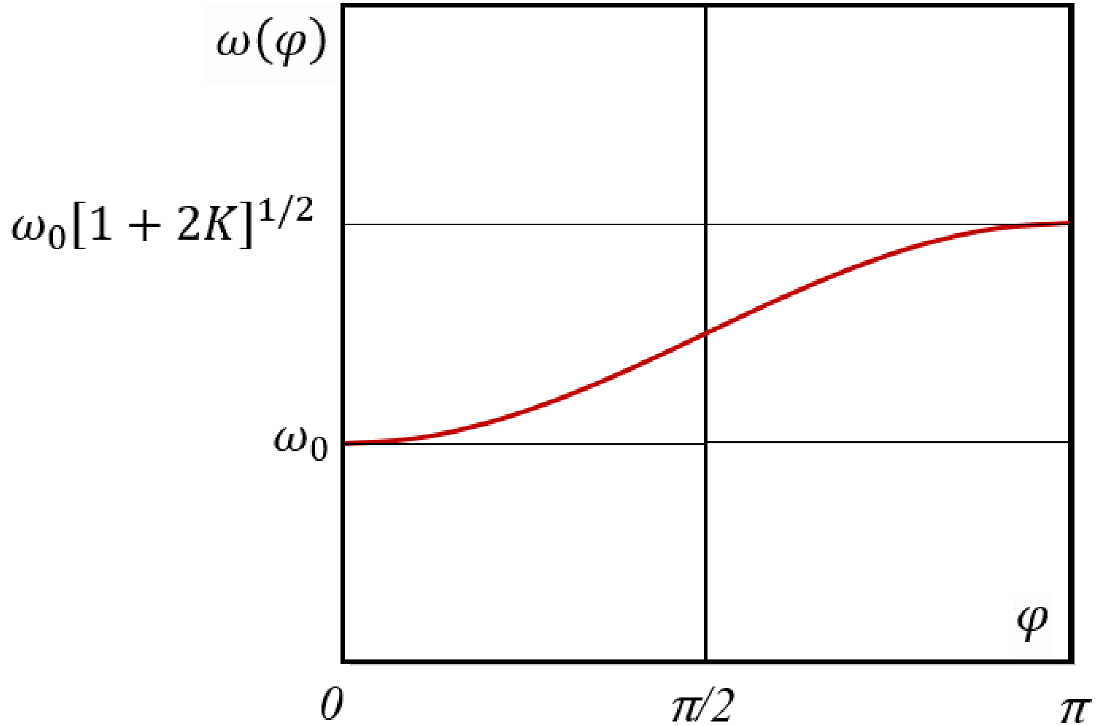

- For small K we have:

$$\omega(\varphi) \approx \omega_0[1+\frac{1}{2}K(1-cos\varphi)]$$

- One can see that

$$K = \frac{\omega(\pi)-\omega(0)}{\omega(0)}$$ - a coupling coefficient; here $\omega(\pi) \approx \omega_0$(1+K), $\omega(0) \approx \omega_0$

$\Delta f = f(\pi) - f(0)$ - a passband width

Travelling–Wave acceleration structures:

- In the arbitrary infinitely long periodic structure, or in the finite structure matched on the ends, there are travelling waves (TW) having arbitrary phase shift per cell φ. Longitudinal wavenumber, therefore, is $k_z = \varphi/d$. Dispersion equation is the same:

$$\omega(k_z) \approx \omega_{\pi/2}\left(1 - \frac{K}{2}cos(\varphi)\right) = \omega_{\pi/2}\left(1 - \frac{K}{2}cos(k_z d)\right)$$

Therefore, the phase velocity $v(\varphi)$ is:

$$v_{ph}(\varphi) = \frac{\omega(k_z)}{k_z} = c\frac{2\pi d}{\varphi\lambda}$$

- For acceleration of the particle having velocity $v_p = \beta c$, the cavity cell length d should be equal to

$$d = \frac{\beta\lambda\varphi}{2\pi},$$

because for synchronism we need $v_p = v_{ph}$

For example, for $\varphi = \pi$ the cell should have the length of $\beta\lambda/2$.

Travelling–Wave acceleration structures:

- The group velocity* $v_{gr}(\varphi)$ is

$$v_{gr}(\varphi) = \frac{d\omega}{dk_z} \approx c\frac{\pi K d}{\lambda} sin(\varphi)$$

For $\varphi=0$ and $\varphi=\pi$ group velocity is zero!

For $\varphi=\pi/2$ group velocity is maximal:

$$v_{gr}(\pi/2) = c\frac{\pi K d}{\lambda}.$$

- For small K group velocity is small compared to the speed of light.

- In contrast to a waveguide, $v_{ph} \cdot v_{gr} \neq c^2$.

*In homogeneous media $v_{gr} = \frac{P}{w}$, P is power flow density, w is energy density.

Travelling–Wave acceleration structures :

John Stewart Bell

- For TW in a periodic structure:

- Average stored energy per unit length for electric field w_E is equal to the average stored energy per unit length for magnetic field w_H (the 1st Bell Theorem*):

$$w_E = w_H = w/2$$

- The power P flow is a product of the average stored energy per unit length and the group velocity (the 2d Bell Theorem*):

$$P = v_{gr} w.$$

***J.S. Bell, "Group velocity and energy velocity in periodic waveguides," Harwell, AERE-T-R-858 (1952). See proof in Appendix 11**

Travelling–Wave acceleration structures

Equivalent circuit:

Note that the electrodynamics in the periodic structure is described by the equivalent circuit

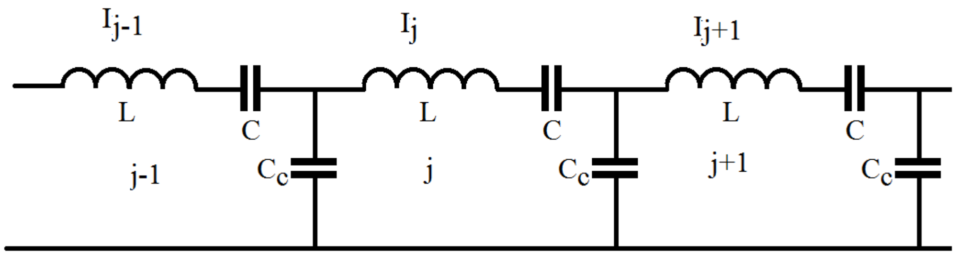

For j[th] cell we have from Kirchhoff theorem:

$$\left(i\omega L + \frac{1}{i\omega C}\right) I_j + \frac{(I_j - I_{j-1})}{i\omega C_c} + \frac{(I_j - I_{j+1})}{i\omega C_c} = 0,$$

For the capacity voltage $X_j = \frac{I_j}{i\omega C}$ we have the same equation as for EM model:

$$X_j \left[1 - (1+K)\frac{\omega_0^2}{\omega^2}\right] + \tfrac{1}{2}K\frac{\omega_0^2}{\omega^2}\left[X_{j-1} + X_{j+1}\right] = 0$$

Here $\omega_0^2 = \frac{1}{LC}$, $K = \frac{2C}{C_c}$, $C = \frac{2}{\omega_0 R/Q}$, $L = \frac{R/Q}{2\omega_0}$.

Travelling–Wave acceleration structures

Loss in the cells:

Ohmic loss on the metallic surface:

$$\omega_0 \to \omega_0\left(1+\frac{i}{2Q_0}\right)$$

$$\vec{E},\vec{H} \sim e^{i\omega_0 t - t/\tau} = e^{i\omega_0 t\left(1+\frac{i}{2Q_0}\right)}$$

$$\tau = \frac{2Q_0}{\omega_0}$$

and

$$X_j\left[1-(1+K)\frac{\omega_0^2}{\omega^2}+i\frac{\omega_0^2}{Q_0\omega^2}\right]+\frac{1}{2}K\frac{\omega_0^2}{\omega^2}\left[X_{j-1}+X_{j+1}\right]=0$$

Equivalent circuit is the following:

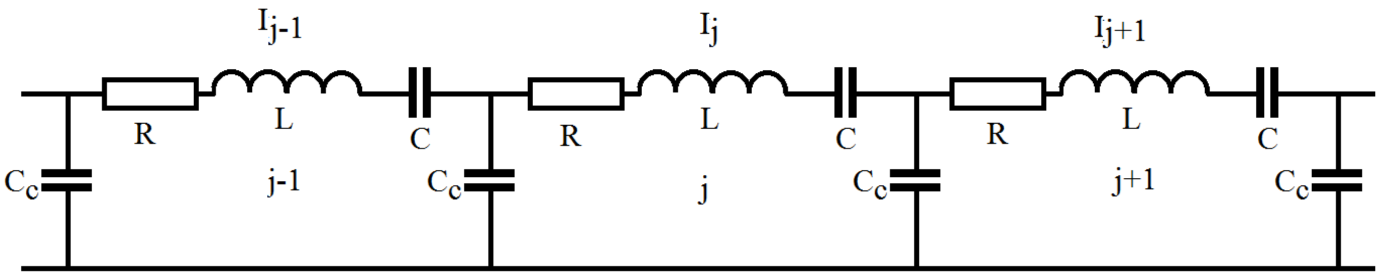

where

$$R = \frac{R/Q}{2Q_0} \qquad \omega_0^2 = \frac{1}{LC},\ \ K = \frac{2C}{C_c},\ C = \frac{2}{\omega_0 R/Q},\ L = \frac{R/Q}{2\omega_0}.$$

Travelling–Wave acceleration structures

However, in a long periodic TW structure Ohmic losses change acceleration field distribution along the structure.

Energy conservation law in the j^{th} cell:

$$\frac{dW_{0,j}}{dt} = -P_j + P_{j-1} - \frac{\omega_0 W_{0,j}}{Q_0},$$

Taking into account that $w = \frac{W_0}{d}$ and $P = w \cdot v_{gr}$ we have

$$\frac{\partial w}{\partial t} = -\frac{\left(w \cdot v_{gr}|_j - w \cdot v_{gr}|_{j-1}\right)}{d} - \frac{\omega_0 w}{Q_0} \approx -\frac{\partial (w v_{gr})}{\partial z} - \frac{\omega_0 w}{Q_0}$$

In steady-state case we have $\frac{dw}{dz} = -\frac{w}{v_{gr}}\left(\frac{dv_{gr}}{dz} + \frac{\omega_0}{Q_0}\right)$

- Constant impedance (CI) structure:

$$v_{gr} = const \rightarrow w(z) = w(0)e^{-\frac{z\omega_0}{v_{gr}Q_0}} \rightarrow E(z) = E(0)e^{-\frac{z}{v_{gr}\tau}} \qquad \tau = \frac{2Q_0}{\omega_0}$$

- Constant gradient (CG) structure:

$$v_{gr}(z) = v_{gr}(0) - z\frac{\omega_0}{Q_0} \rightarrow w(z) = w(0) \rightarrow E(z) = E(0) = const$$

Aperture a should decrease with z.

Travelling–Wave acceleration structures

Tolerances:
If the cell frequencies have resonant frequency deviation $\delta\omega_0$, it changes the longitudinal wave number k_z and violates synchronism.

$$\delta k_z = \frac{dk_z}{d\omega_0}\delta\omega_0 = \frac{1}{v_{gr}}\delta\omega_0$$

It means that it is necessary to operate in the middle of dispersion curve, when group velocity is maximal, $\varphi \sim \pi/2 - 2\pi/3$.

If φ close to π, the structure is unstable.

Travelling–Wave acceleration structures

TW structure parameters:
For TW stricture R and R/Q are calculated per unit length of the structure.

- Shunt impedance R is measured in MOhm/m. For geometrically similar cells R scales as $\omega_0^{1/2}$.
- R/Q is measured in Ohm/m. For geometrically similar cells R/Q scales as ω_0

Travelling–Wave acceleration structures

TW structure parameters: *(R/Q)* for pillbox, f=10 GHz (here b is the cavity radius)

$$\frac{R}{Q} = \frac{0.98 Z_0 T(\psi)^2}{b}, \qquad b = \frac{2.405c}{2\pi f}$$

(See Lecture 11, slide 58)

R/Q, Ohm/m

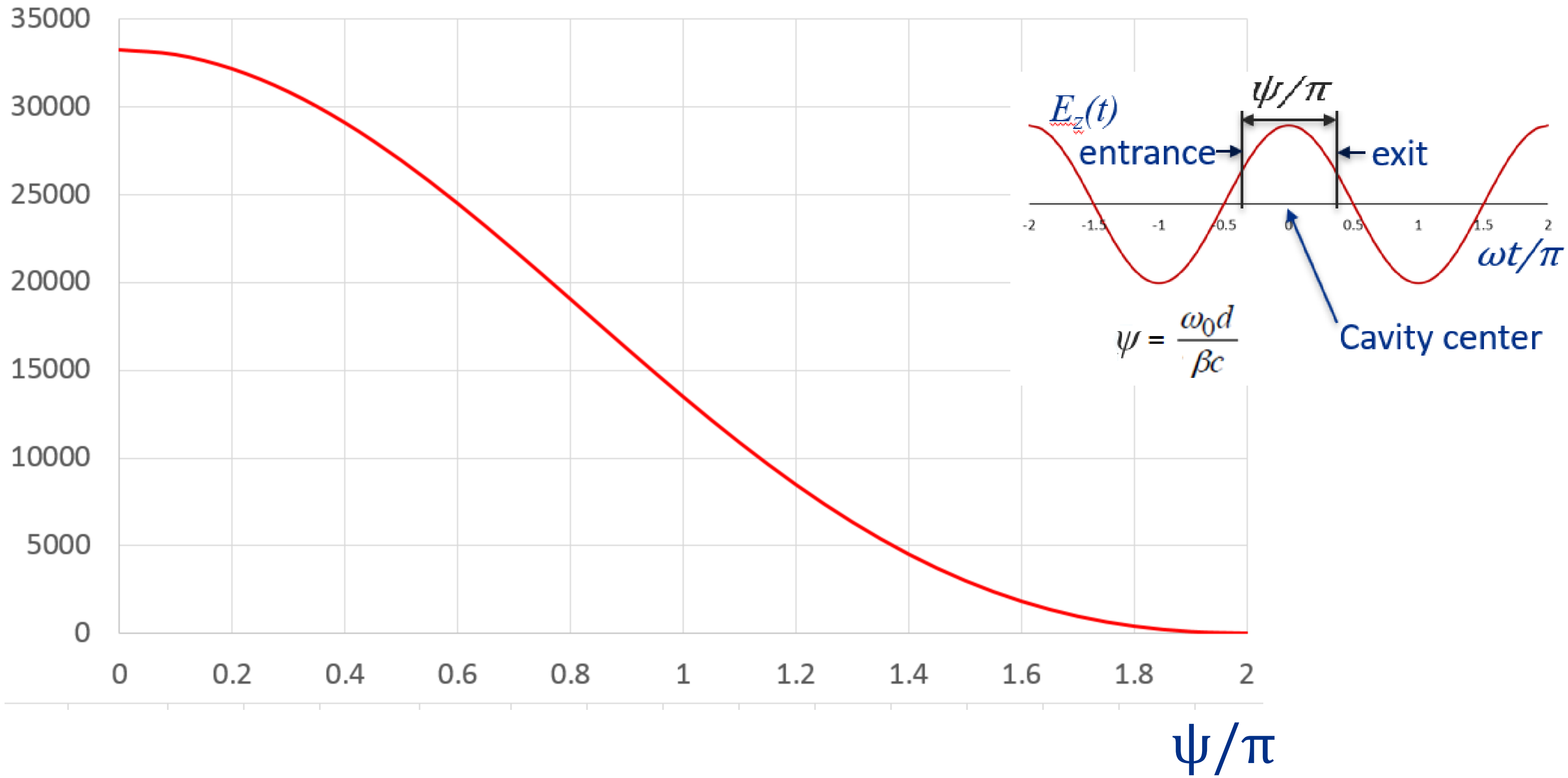

Travelling–Wave acceleration structures

TW structure parameters: Q_0 for pillbox at 10 GHz (see Lecture 11, slide 53)

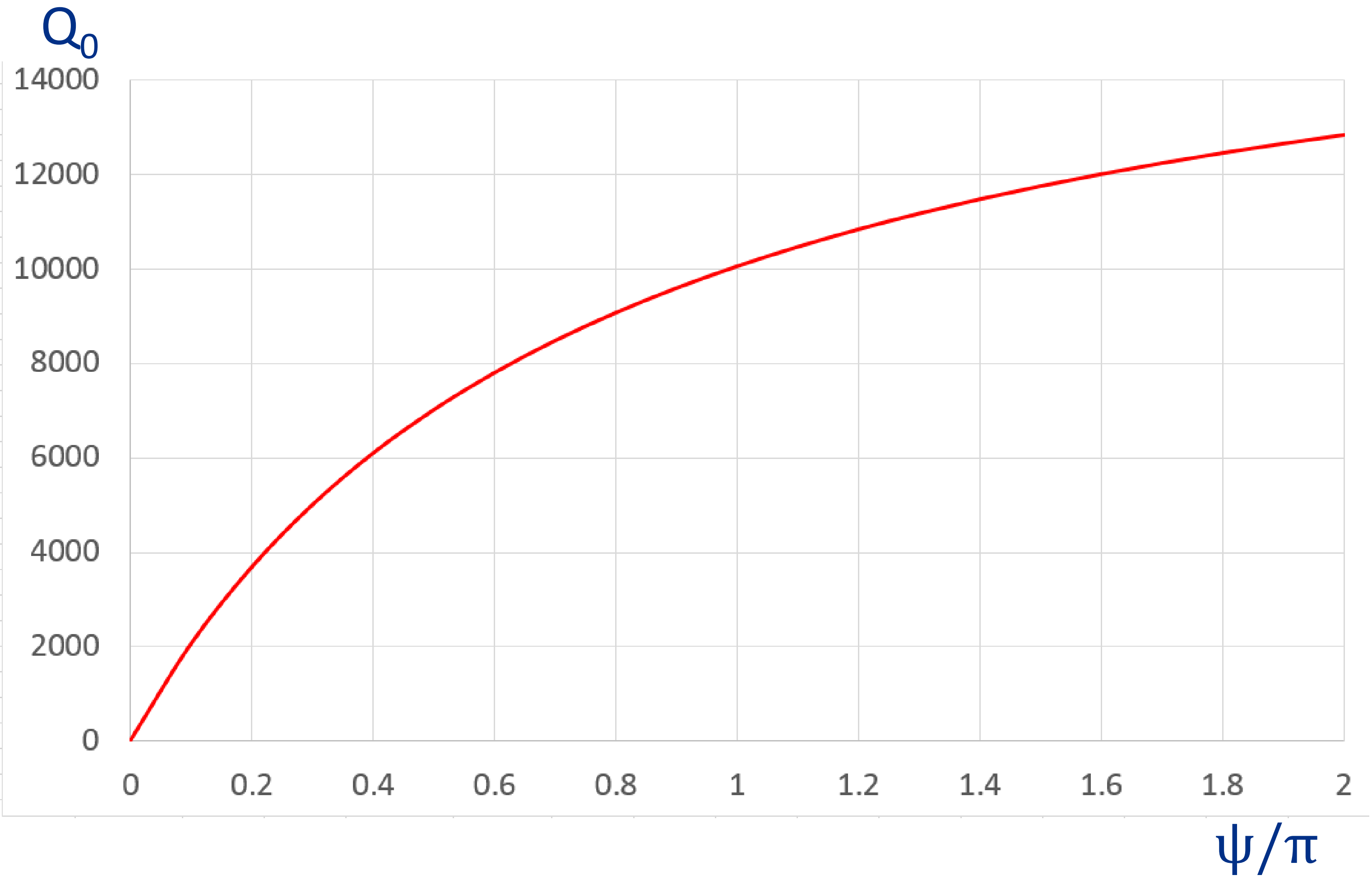

Travelling–Wave acceleration structures

TW structure parameters: Shunt impedance $R=(R/Q)\cdot Q_0$ for pillbox at 10 GHz

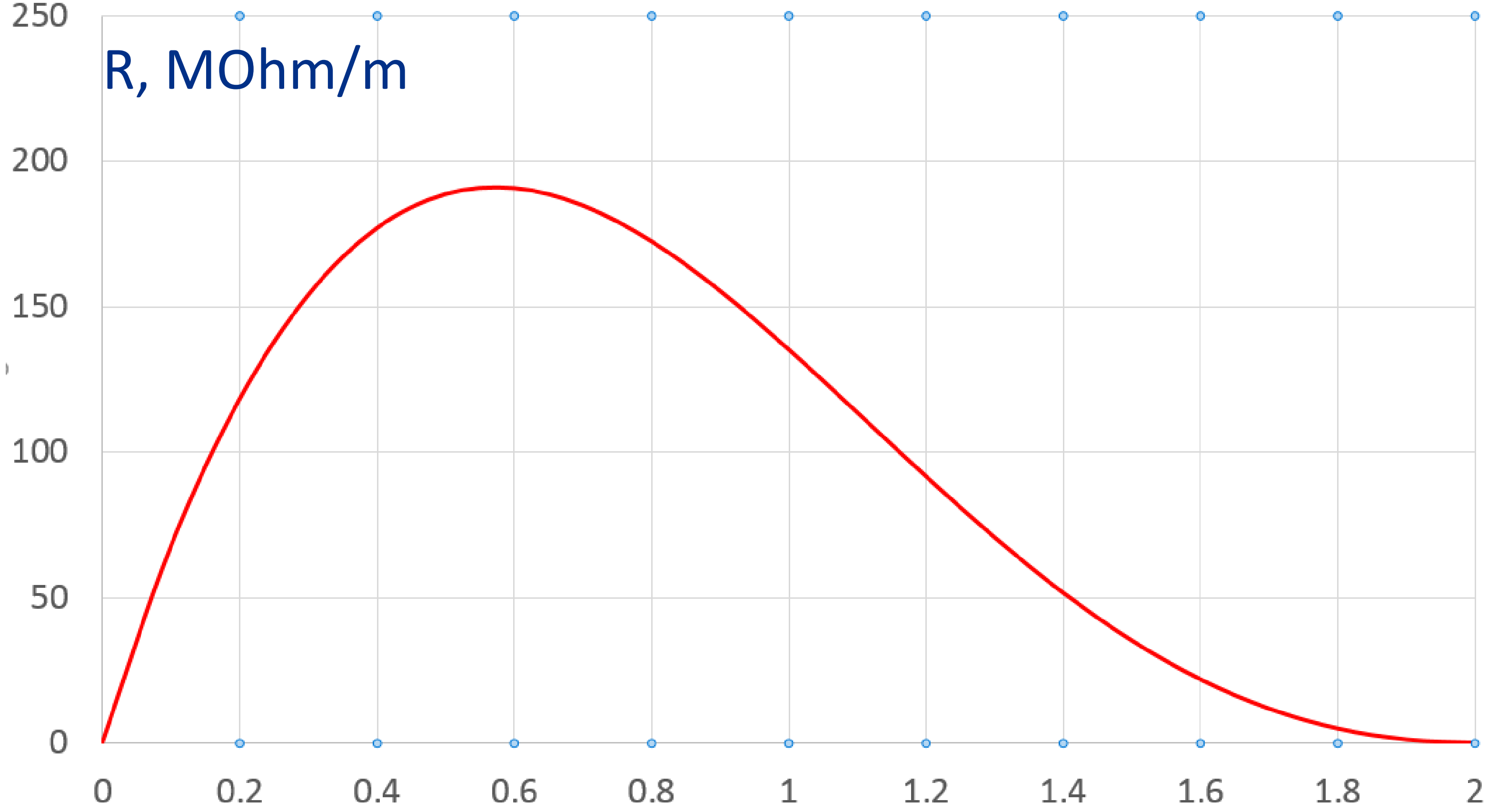

R is maximal at ψ ~ 0.6π. Typically, they use ψ =2π/3. ψ/π

Travelling–Wave acceleration structures

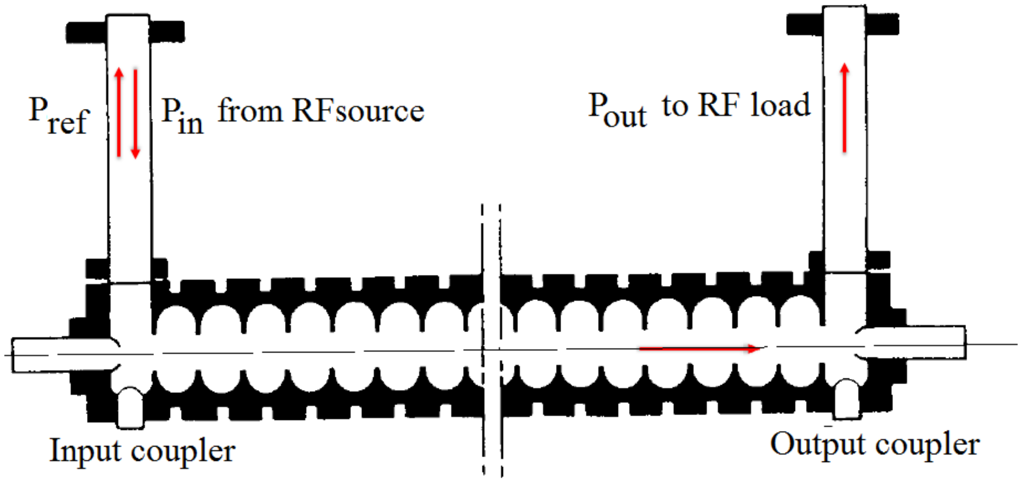

$$P_{in} = P_{ref} + P_{out} + P_{loss} + P_{beam}$$
$$P_{in} >> P_{out}$$

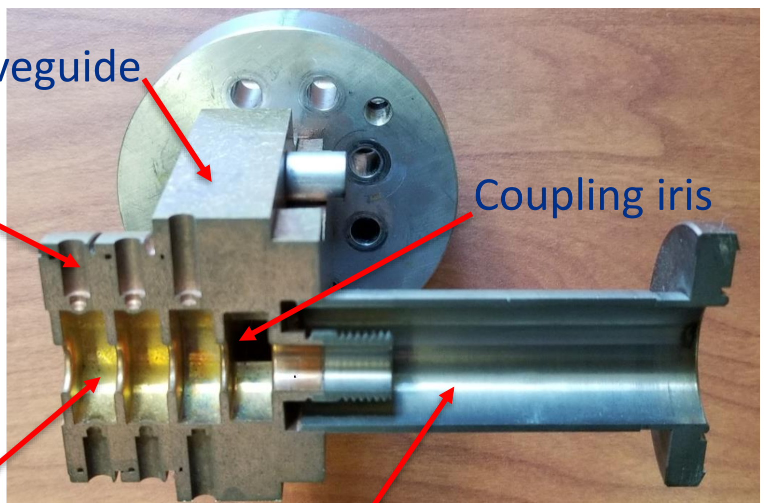

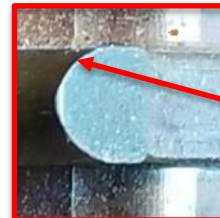

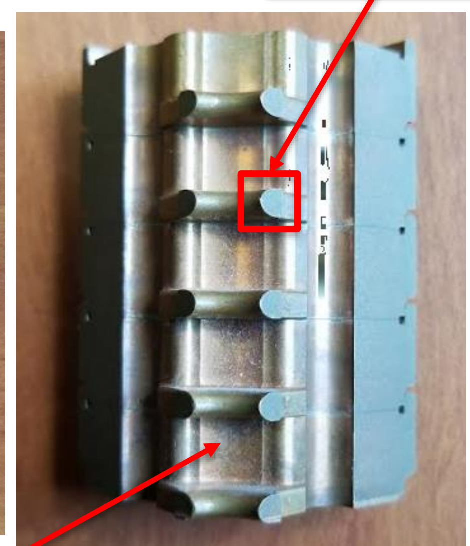

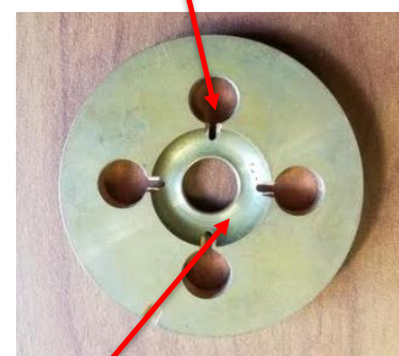

NLC structure with HOM damping

Travelling–Wave acceleration structures

TW structures for acceleration of electrons are widely used is different fields.

- **High – energy physics:**
  - SLAC (1968): 3 km, 47 GeV (max), 2π/3 2.856 GHz (S-band) , 3 m structures.
  - SLC (1987) – first e^+e^- linear collider based on the SLAC linac.
  - CLIC collider (R&D): up to 50 km, up to 3 TeV c.m., 2π/3 12 GHz
- **FELS:**
  - SwissFEL (PSI) 5.7 GHz linac (2017), 0.74 km, 5.8 GeV, 2π/3 6 GHz
- **Industrial and medical accelerators**
  - Varian S-band (2.856 GHz) and X-band (11.424 GHz) linacs for medical applications
  - Industrial linacs

Travelling–Wave acceleration structures

Modern TW structures: 12 GHz CLIC structure*

Accelerating structure parameters

Loaded gradient* [MV/m]	100
Working frequency [GHz]	11.994
Phase advance per cell	$2\pi/3$
Active structure length [mm]	217
Input/output radii [mm]	3.15/2.35
Input/output iris thickness [mm]	1.67/1.00
Q factor [Cu]	7112/7445
Group velocity [%c]	1.99/1.06
Shunt impendence [MΩ/m]	107/137
Peak input power [MW]	60.9
Filling time [ns]	49.5
Maximum E-field [MV/m]	313
Maximum modified Poynting vector[MW/mm^2]	7.09
Maximum pluse heating temperature rise [K]	35

*V. Dolgashev, SLAC, EAAC 2015

Travelling–Wave acceleration structures

Modern TW structures: 12 GHz CLIC structure*

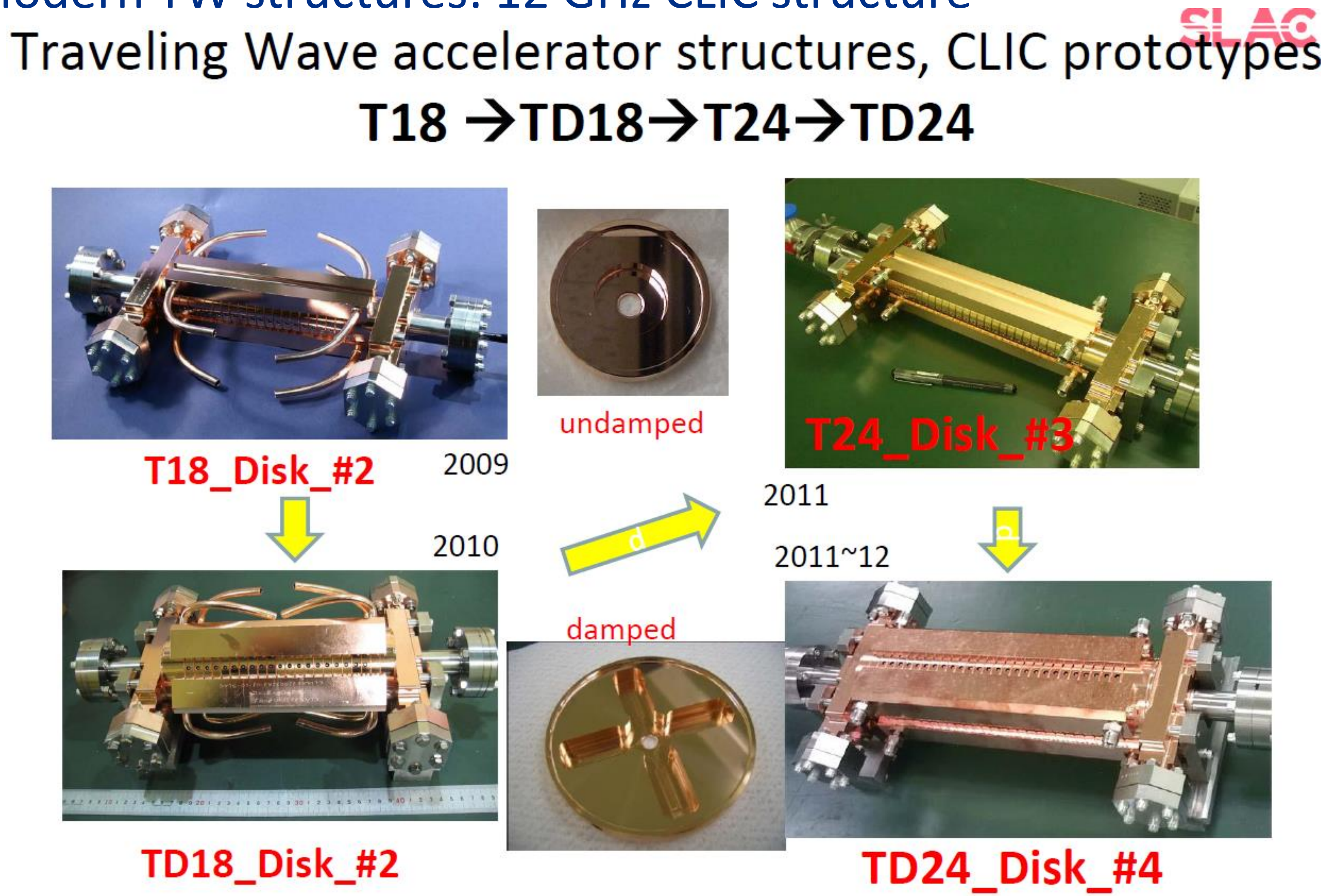

Travelling–Wave acceleration structures

Modern TW structures: 12 GHz CLIC structure*

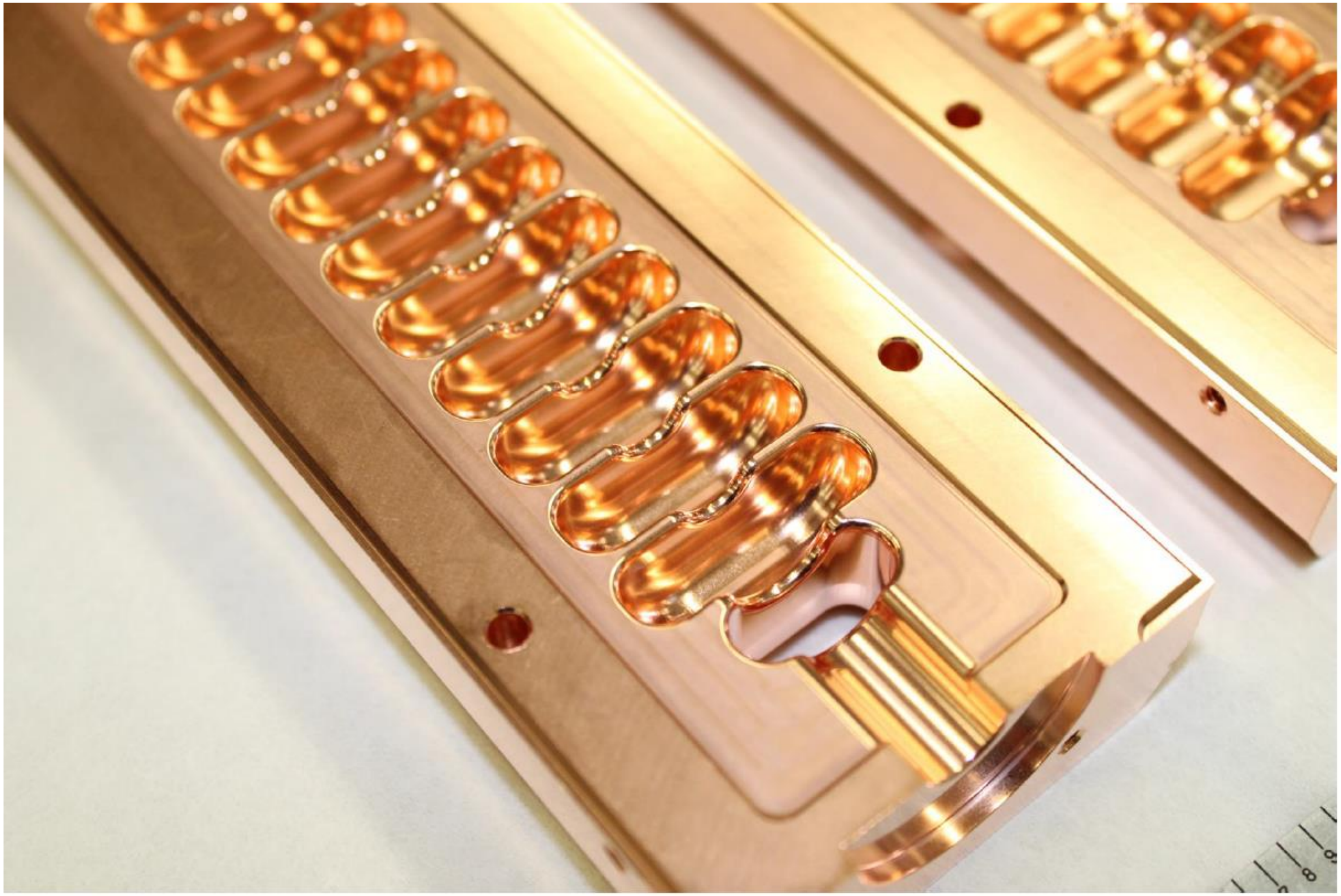

SLAC-CERN

Travelling–Wave acceleration structures

Final beadpull of tuned CLIC-G-OPEN

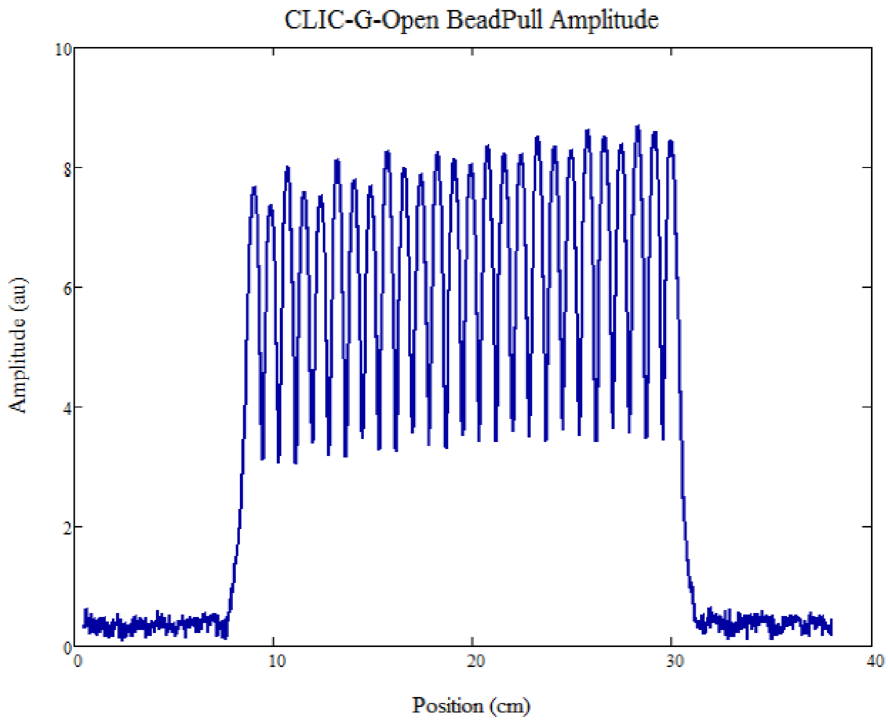

On-axis field amplitude.

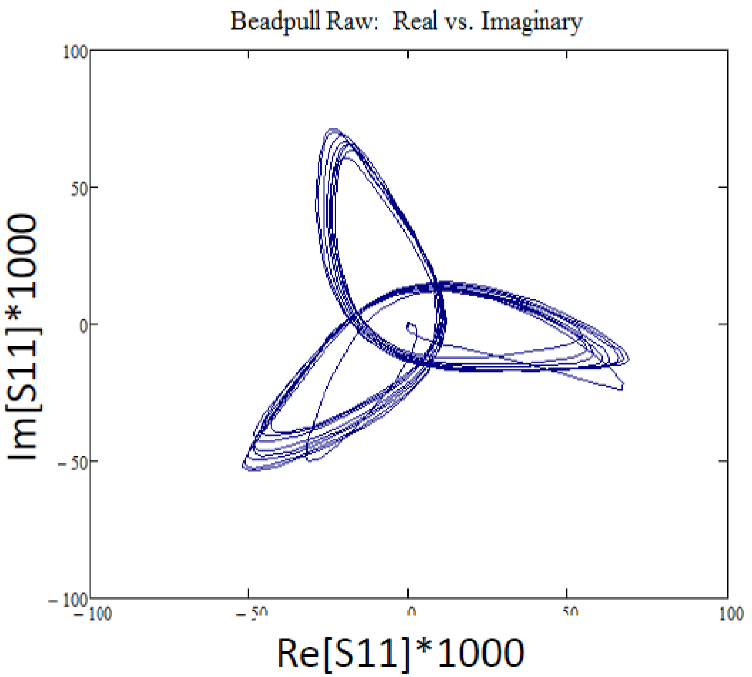

Polar plot of beadpull data.

Travelling–Wave acceleration structures

Output Part of the Open 100 GHz Copper Traveling Wave Accelerating Structure

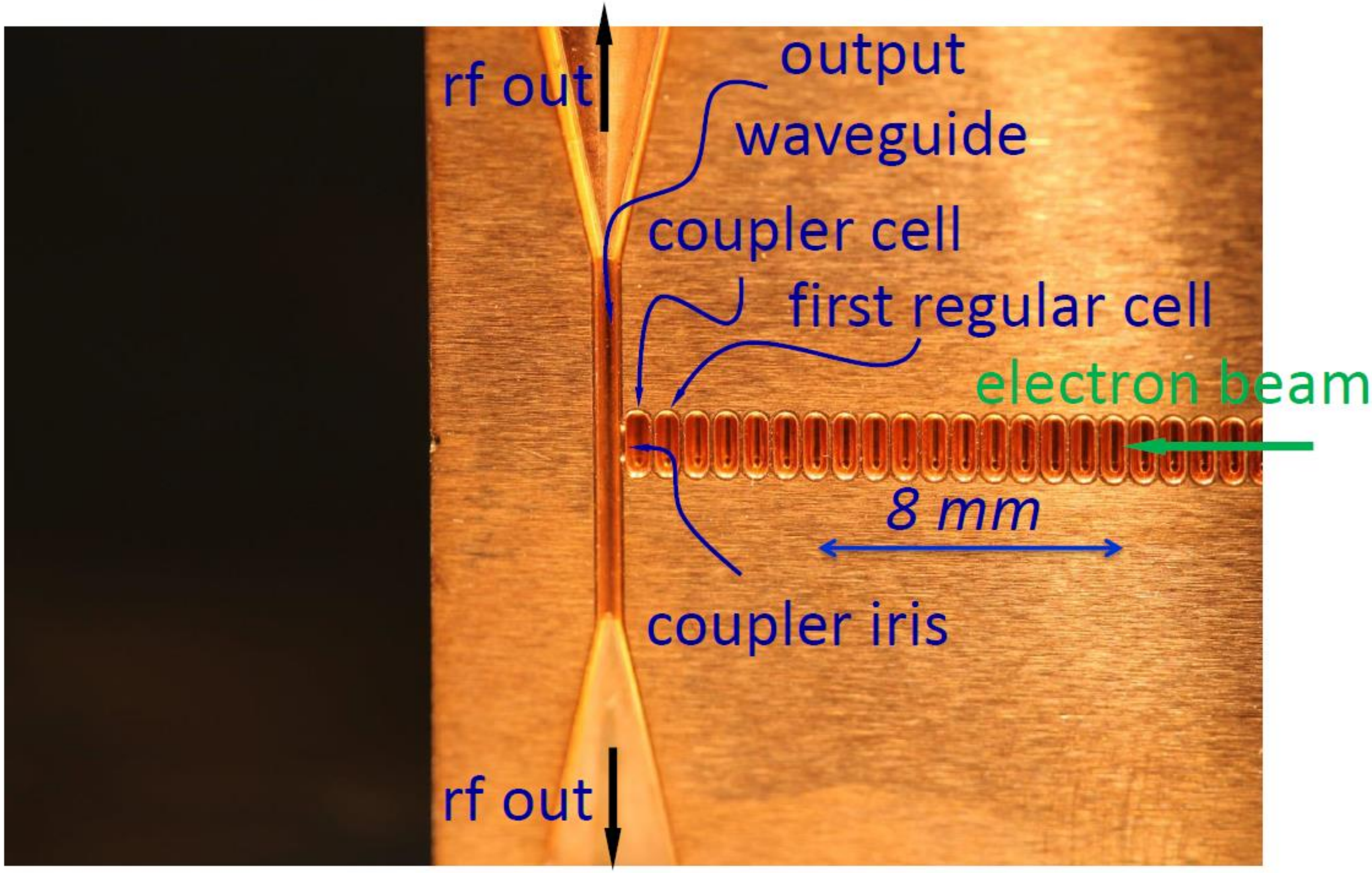

SLAC-INFN

Summary:

- Single – cell cavities are not convenient in order to achieve high acceleration: a lot of couplers, tuners, etc. Especially it is important for acceleration of electrons.
- Periodic structures are used for acceleration, where travelling wave is excited.
- Phase velocity depend on the phase advance per cell. The accelerating wave has the same phase velocity as the accelerated particles (synchronism).
- Average energy of magnetic field is equal to average energy of electric field (the 1st Bell theorem); Power flaw is equal to the product of the group velocity to the average stored energy per unit length (the 2d Bell theorem).
- The passband depends on the value of coupling between the cells K ; it depends on the coupling hole radius a as ~ a^3-a^4; it depends also on the wall thickness.
- Group velocity is maximal if phase advance per cell is ~$\pi/2$;
- Maximal shunt impedance per unit length is at the phase shift of ~$2\pi/3$;
- Loss may change the field distribution. To achieve field flatness along the structure, group velocity (coupling) should decrease from the structure beginning to the end.

Chapter 5.

Standing –Wave acceleration structures.

a. Standing - wave structures;
b. Equivalent circuit for a SW structure;
c. Dispersion curve;
d. Normal modes;
e. Perturbation theory for SW structures;
e. Parameters of SW structures;
f. Bi-periodic SW structures;
g. Inductive coupling;
h. Types of the SW structures;

Standing–Wave acceleration structures

- **TW structures work very good for RT electron accelerators:**
- High frequency → lower power ($R \sim f^{1/2}$);
- A lot of cells (many tens) → high efficiency (all the power is consumed in the structure, and small fraction is radiated through the output port).
- **TW structures are not good for RT proton accelerators:**
- High frequency is not practical (defocusing is proportional to f)
- Low beam loading → large number of cells (impractical from the point of view of focusing and manufacturing, especially if the cell diameter is large because of low frequency);
- **TW structures are not good for SRF accelerators:**
- High frequency is not practical (BCS surface resistance is proportional to f^2)
- Small decay in the cavities
  - Very large number of cells + large cell size (impractical from the point of view of manufacturing and processing);
  - Feedback waveguide - still under R&D

Fermilab & Euclid 3-cell SRF TW structure prototype

Standing–Wave acceleration structures

Standing Wave structures:

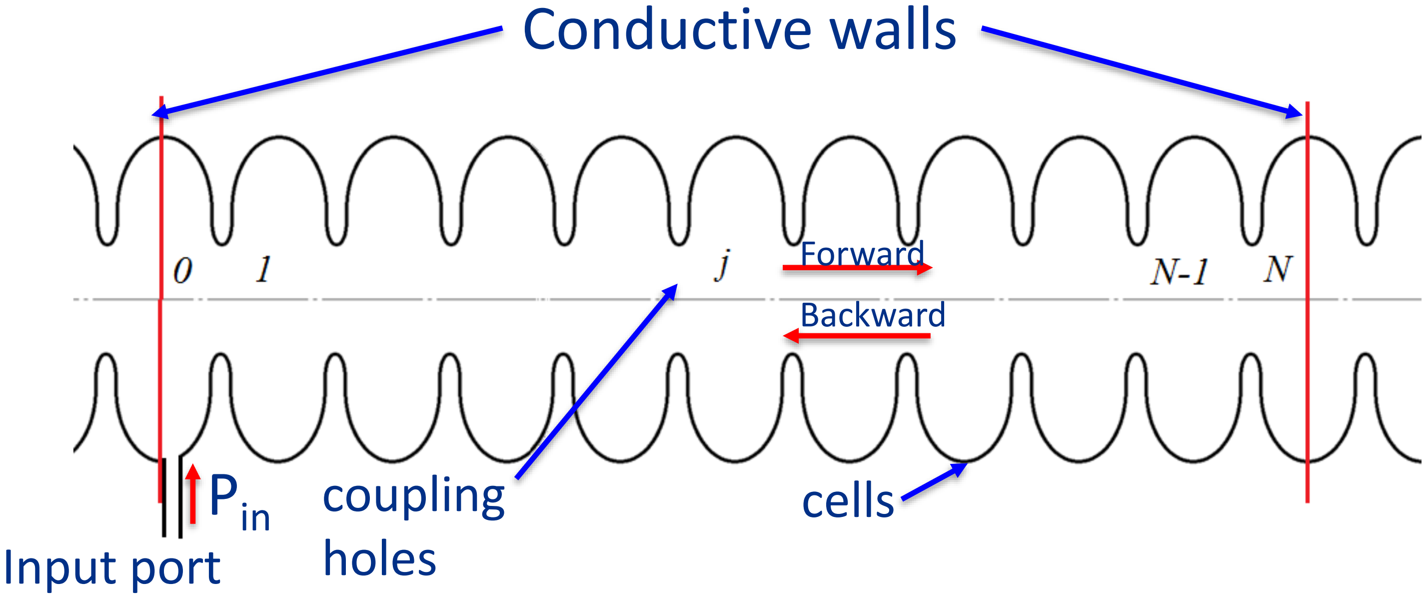

Putting reflective conductive walls in the middle of the end cells, we do not violate boundary conditions for EM field for TM_{010}-like modes.

Forward and backward travelling waves form standing wave.

- N may be small, even $N=2$;
- Frequency may be small, up to hundreds of MHz→ proton acceleration
- Suitable for SRF
- $P_{in} << P_{forward} \approx P_{backward}$

Standing–Wave acceleration structures

Equivalent circuit of the SW structure containing half-cells on the ends:

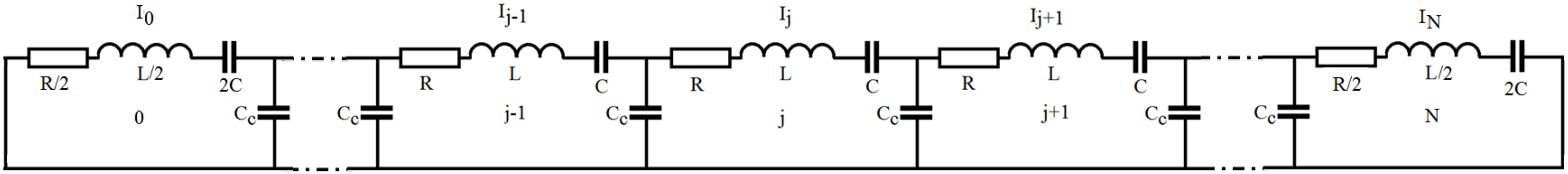

$$X_0\left[1-\frac{\omega_0^2}{\omega^2}+i\frac{\omega_0^2}{Q_0\omega^2}\right]+K\frac{\omega_0^2}{\omega^2}X_1=0$$

$$X_j\left[1-\frac{\omega_0^2}{\omega^2}+i\frac{\omega_0^2}{Q_0\omega^2}\right]+\frac{1}{2}K\frac{\omega_0^2}{\omega^2}\left[X_{j-1}+X_{j+1}\right]=0 \quad (1)$$

$$X_N\left[1-\frac{\omega_0^2}{\omega^2}+i\frac{\omega_0^2}{Q_0\omega^2}\right]+K\frac{\omega_0^2}{\omega^2}X_{N-1}=0$$

In matrix form:

$$M\hat{X}-\frac{\omega_0^2}{\omega^2}\hat{X}=0$$

here $M_{jj}=1;\ j=0,1,\dots N;$

$$M_{jj-1}=\frac{K}{2W(j)};\ j=1,2,\dots N;$$

$$M_{jj+1}=\frac{K}{2W(i)};\ j=0,1,\dots N-1.$$

and $W(j)=1, j=1,2,\dots N-1$

$$W(j)=\frac{1}{2}, j=0,N$$

Here ω_0 corresponds to the center of dispersion curve.

Fermilab

Standing –Wave acceleration structures

Eigenvectors and eigenvalues:

$$\hat{X}_j^q = cos\frac{\pi qj}{N};\ \omega_q^2 = \frac{\omega_0^2}{1 + Kcos\frac{\pi q}{N}}, q = 0,1, \dots N$$

Phase advance per cell: $\varphi = \frac{\pi q}{N}, q = 0,1,..N$

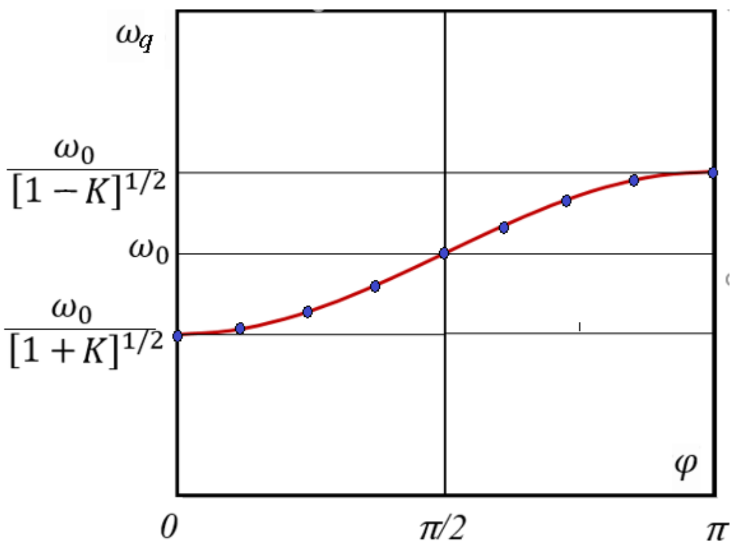

3-cell cavity (N=2)

0-mode (q=0):

$\varphi = 0 \quad \omega = \frac{\omega_0}{(1-K)^{1/2}}$

π/2-mode (q=1):

$\varphi = \pi/2 \quad \omega = \omega_0$

Even cell is empty!

π-mode (q=2):

$\varphi = \pi \quad \omega = \frac{\omega_0}{(1+K)^{1/2}}$

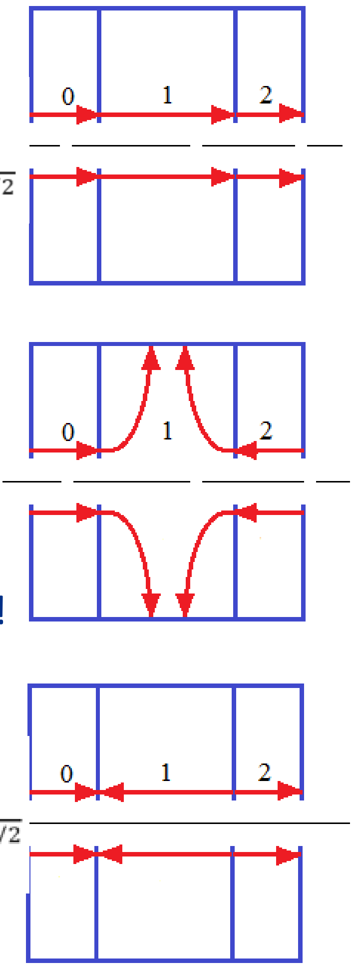

Orthogonality:

$$\hat{X}^q \cdot \hat{X}^r \equiv \sum_{j=0}^{N} W(j)\, \hat{X}_j^q \hat{X}_j^r = \frac{N\delta_{qr}}{2W(q)},\quad \delta_{qq} = 1, and\ \delta_{qr} = 0, if\ q \neq r$$

Standing –Wave acceleration structures

- Perturbation of the cell resonance frequencies causes perturbation of the mode resonance frequencies $\delta\omega_q$;
- the field distribution $\delta\hat{X}_q$.

$$\omega_{0j}^{2\prime} = \omega_0^2 + \delta\omega_{0j}^2 \quad \rightarrow \hat{X}^{q\prime} = \hat{X}^q + \delta\hat{X}^q, \quad \hat{X}^q \cdot \delta\hat{X}^q$$

Variation of the equation (1) in matrix form $M\hat{X} - \frac{\omega_0^2}{\omega^2}\hat{X} = 0$, see Slide 31

gives $M\delta\hat{X}^q = \frac{\omega_0^2}{\omega_q^2}\left[\delta\hat{X}^q + \Omega\hat{X}^q - \frac{\delta\omega_q^2}{\omega_q^2}\hat{X}^q\right],$

(here $\Omega = \begin{bmatrix} \frac{\delta\omega_{01}^2}{\omega_0^2} & \cdots & 0 \\ \vdots & \ddots & \vdots \\ 0 & \cdots & \frac{\delta\omega_{0N}^2}{\omega_0^2} \end{bmatrix}$)

$$\frac{\delta\omega_q^2}{\omega_q^2} = [2W(q)/N] \cdot \hat{X}^q\Omega\hat{X}^q;$$

$$\delta\hat{X}^q = \sum_{q' \neq q} \frac{2W(q')\hat{X}^q\Omega\hat{X}^q}{N\left(\frac{\omega_q^2}{\omega_{q'}^2} - 1\right)}\hat{X}^{q'}$$

$$\left|\delta\hat{X}^q\right| \sim \frac{\left|\delta\omega_{0j}\right|_{av}}{\left|\omega_q - \omega_{q\pm1}\right|}$$

Fermilab

Standing –Wave acceleration structures

π/2-mode ($q=N/2$): N-even, N is the number of cells in the cavity

$$|\delta\hat{X}^{N/2}| \sim \frac{|\delta\omega_{0j}|_{av}}{|\omega_{N/2}-\omega_{N/2-1}|} \sim N\frac{|\delta\omega_{0j}|_{av}/\omega_0}{K}$$

π-mode ($q=N$):

$$|\delta\hat{X}^{N}| \sim \frac{|\delta\omega_{0j}|_{av}}{|\omega_{N}-\omega_{N-1}|} \sim N^2\frac{|\delta\omega_{0j}|_{av}/\omega_0}{K}$$

SW π-mode is much less stable than π/2-mode !

For π-mode problems with

- Tuning
- Temperature stability at RT

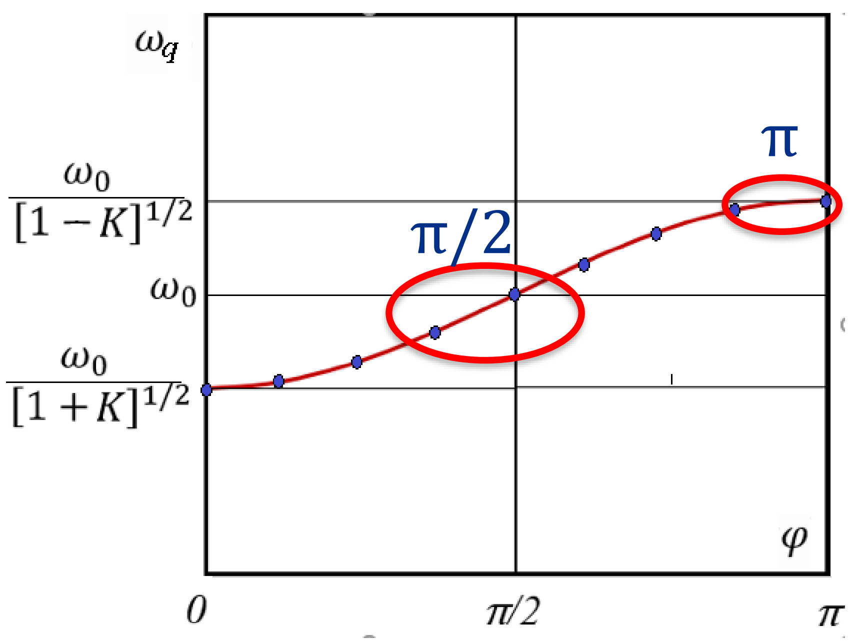

$$\omega_q^2 = \frac{\omega_0^2}{1+K\cos\frac{\pi q}{N}}, q = 0,1, \dots N$$

Fermilab

Standing –Wave acceleration structures

Solutions:

- ❖ Operate at $\pi/2$ mode;
- ❖ Operate at π mode:
  - Small number of cells N;
  - Increase K.

1. Operating at $\pi/2$ mode:

$$\hat{X}_j = \cos\frac{\pi j}{2}$$

Even cells are empty!

Solution – biperiodic structures:

- Narrow even cells (coupling cells)
- Long odd cells (acceleration cells)
- Same length of the period containing 2 cells, $\beta\lambda/2$
- The structure is "$\pi/2$ for RF" and "π for the beam"

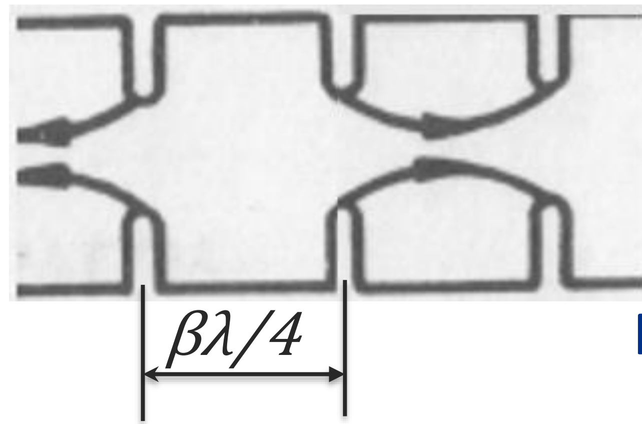

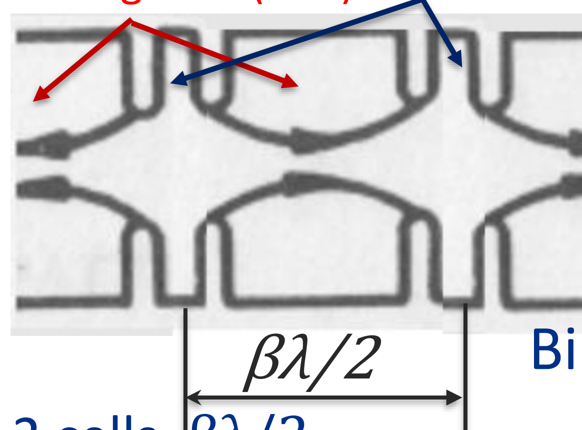

Standing –Wave acceleration structures

2. Increase K:

- Coupling through the aperture holes does not provide high K;
  - Aperture is limited by surface electric field
  - At β<c acceleration gain on the axis drops as $\sim exp\ (ka/\beta)$*
- In this case, R_{sh} is modest (the drift tubes cannot be used)

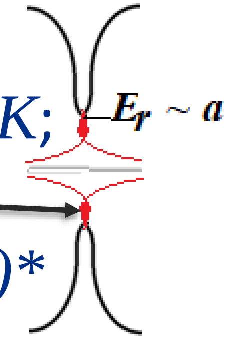

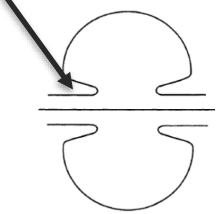

Solution: inductive coupling through the side slots.
Aperture may be small in this case, which provides

- Small field enhancement factors;
- High R/Q and R_{sh}.

Coupling slots

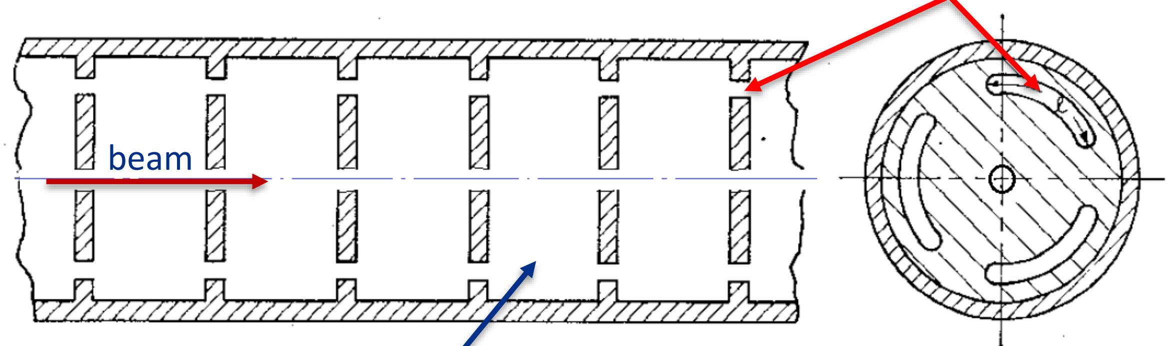

Accelerating cells

*See Lecture 7, slide 25

Standing–Wave acceleration structures

TEM wave in the slot → high electric field → high coupling

Induction coupling gives negative K

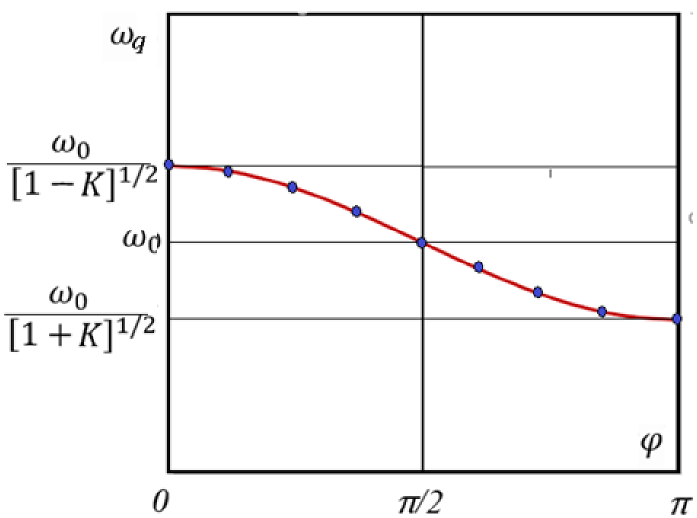

$$K = -\frac{2L_c}{L_c}$$

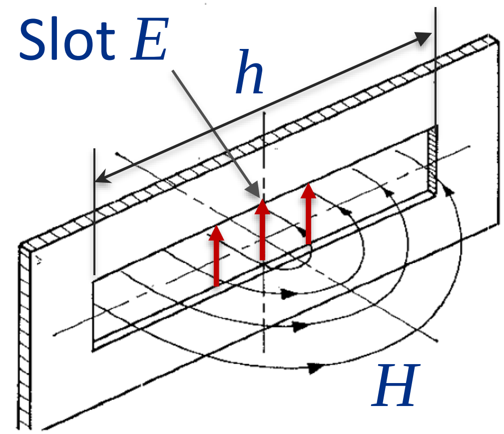

Slot resonance: $h = \lambda/2$. Typically, $h < \lambda/2$

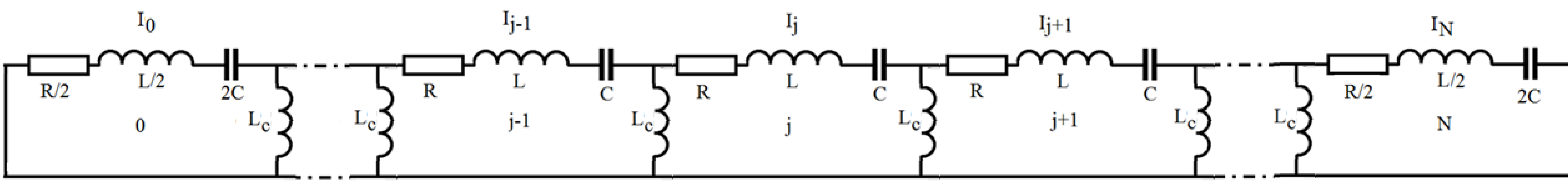

Equivalent circuit below the slot resonance

Standing–Wave acceleration structures

Combination:

- Inductive coupling
- Biperiodic structure

Biperiodic structures with induction coupling

- Coupling cells between accelerating cells

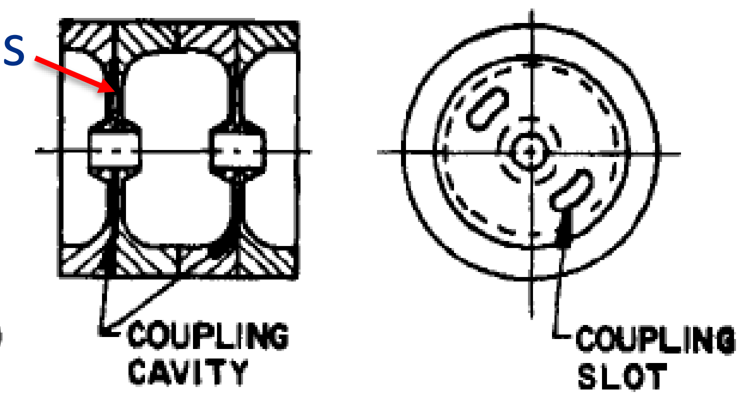

- Side coupling cells

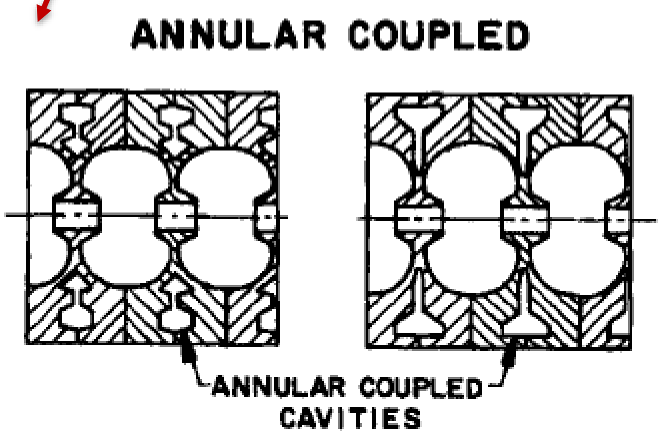

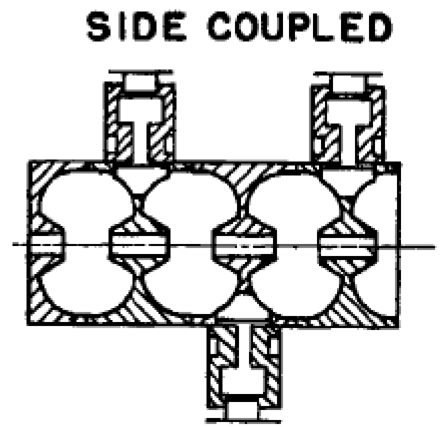

Standing–Wave acceleration structures

Inductive coupling slots cause multipole perturbation of the acceleration field, which may influence the beam dynamics:

$$x'_f = \frac{\Delta p_\perp}{p_{||}} \approx \frac{m}{ka}\left(\frac{V_{max}(a)}{\gamma m_0 c^2}\right)\left(\frac{x_i}{a}\right)^{m-1}$$

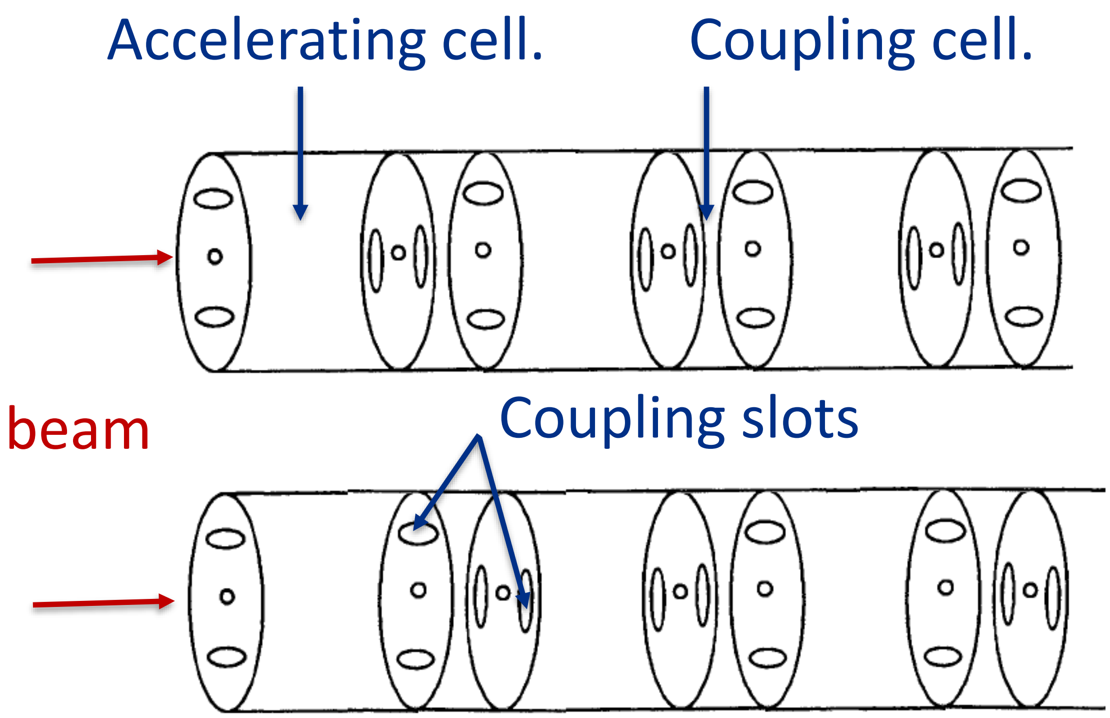

Coupling slot orientation:

Wrong! Strong quadrupole defocusing in one of transverse directions.

Right! Strong quadrupole focusing in both directions.

Standing–Wave acceleration structures

Different types of the RT SW acceleration structures:

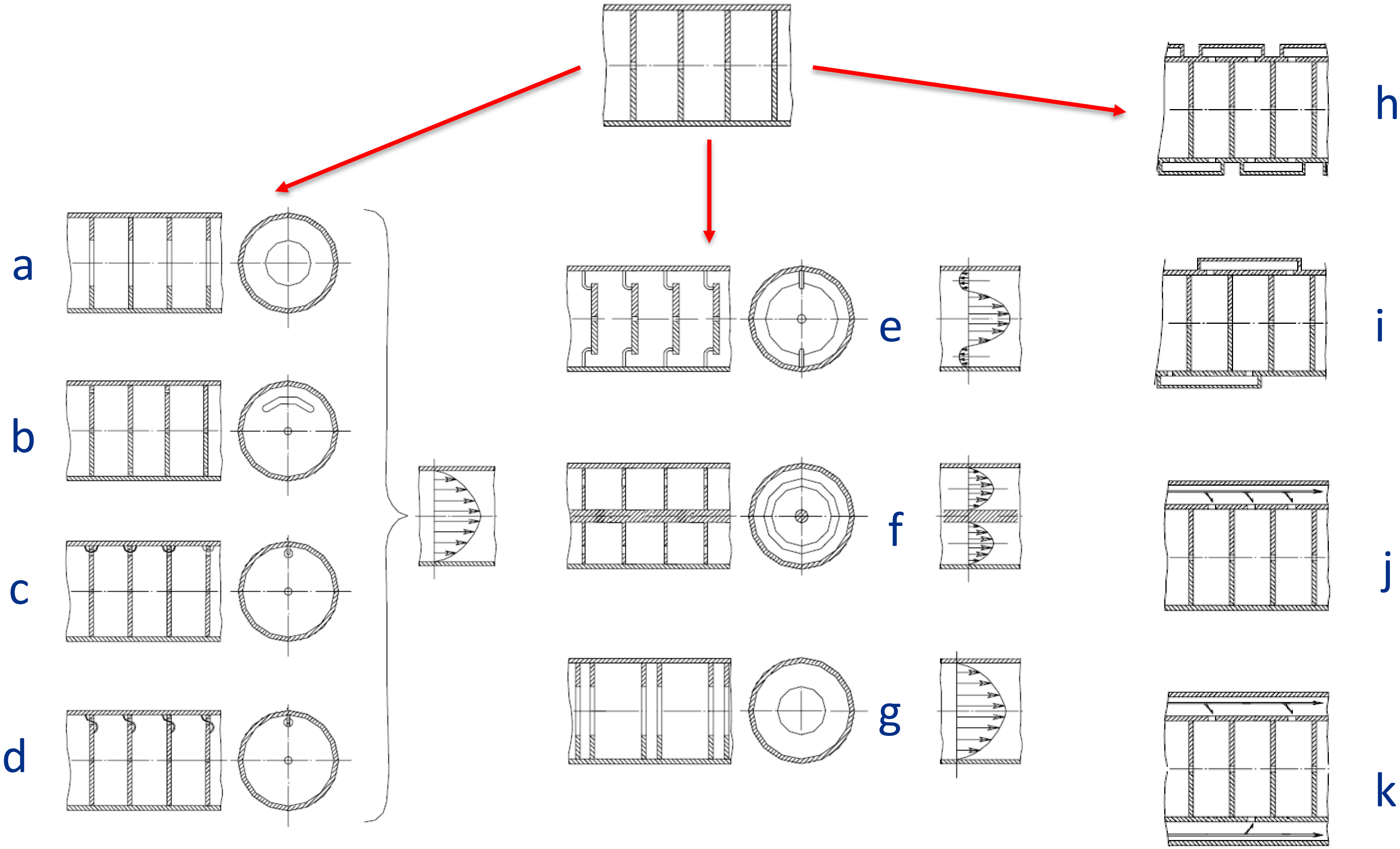

Fermilab

Summary:

- TW structures are not practical for RT proton accelerators (low beam loading.
- TW structures are not practical for SRF accelerators, proton and electron.
- The cure is a standing – wave structure.
- In the SW structure the operating mode is split, the number of resulting modes is equal to the number of cells.
- π/2 - mode is the most stable versus cell frequency perturbation, field distribution perturbation is proportional to the number of cells.
- 0- mode and π- mode are less stable versus cell frequency perturbation, field distribution perturbation is proportional to the number of cells squared, wich does not allow large number of cells.
- Remedy:
  - biperiodic structures;
  - inductive coupling.

Chapter 6.

Why SRF cavities?

Why SRF?

The surface resistance

The radio-frequency surface resistance can be described in terms of three different contributions:

$$R_s(T,\omega,B,l) = R_{BCS}(T,\omega,l) + R_{fl}(B,l) + R_0$$

Where:

$$R_{BCS}(T,\omega,l) \cong \frac{A(l)\omega^2}{T} e^{-\frac{\Delta}{\kappa_B T}}$$

BCS resistance is caused by electron inertia;

$R_{fl}(B,l) \Rightarrow$ trapped flux surface resistance

$R_0 \Rightarrow$ intrinsic residual resistance, due to:

i. Sub-gap states
ii. Niobium hydrides
iii. Damaged layer
iv. ...

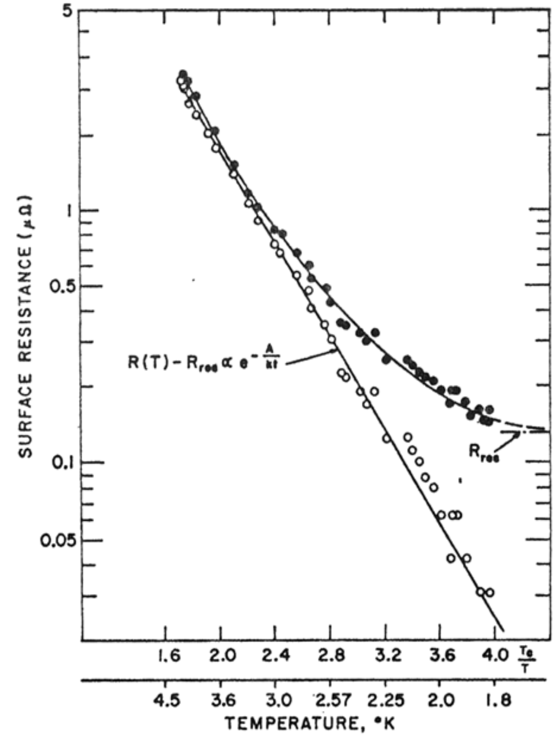

J. R. Delayen, SRF1987

Type-II superconductors

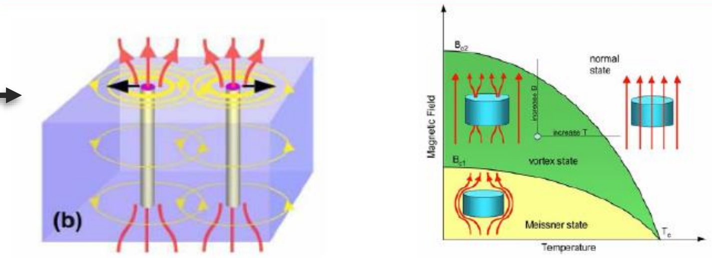

Main thermodynamic parameters of type-II superconductors:

1. Critical temperature, T_c
2. Lower critical field H_{c1}
3. Upper critical field H_{c2}

Why SRF?

- For copper cavity at RT (σ = 5.96e7 S/m) for f=1.3 GHz one has R_s = 9.5 mOhm.
- For SRF Nb cavity at 2K on has R_s = 8.5 nOhm (ILC –type cavity, electropolishing),

It is 1.e6 times less!

Therefore, CW and high Duty Factor are possible at high gradient, even taking into account “conversion factor” for heat removal at 2K (~1000-1200W/W)

Why SRF?

RT: Q_0 ~1e4 SRF: Q_0 ~1e10

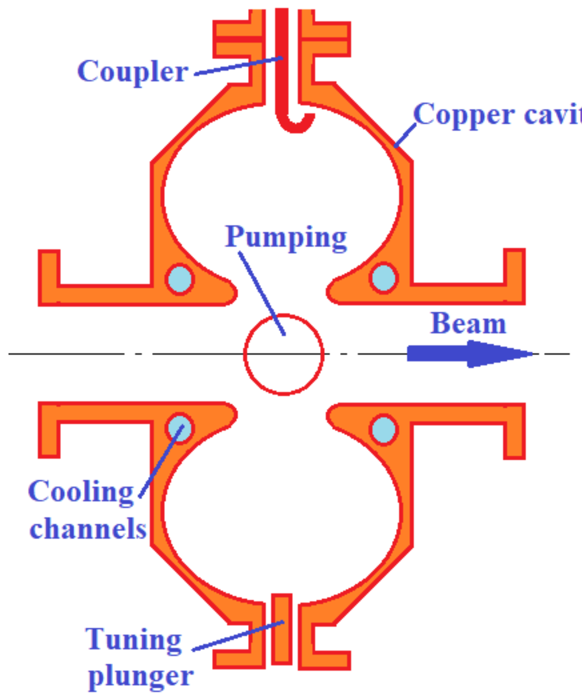

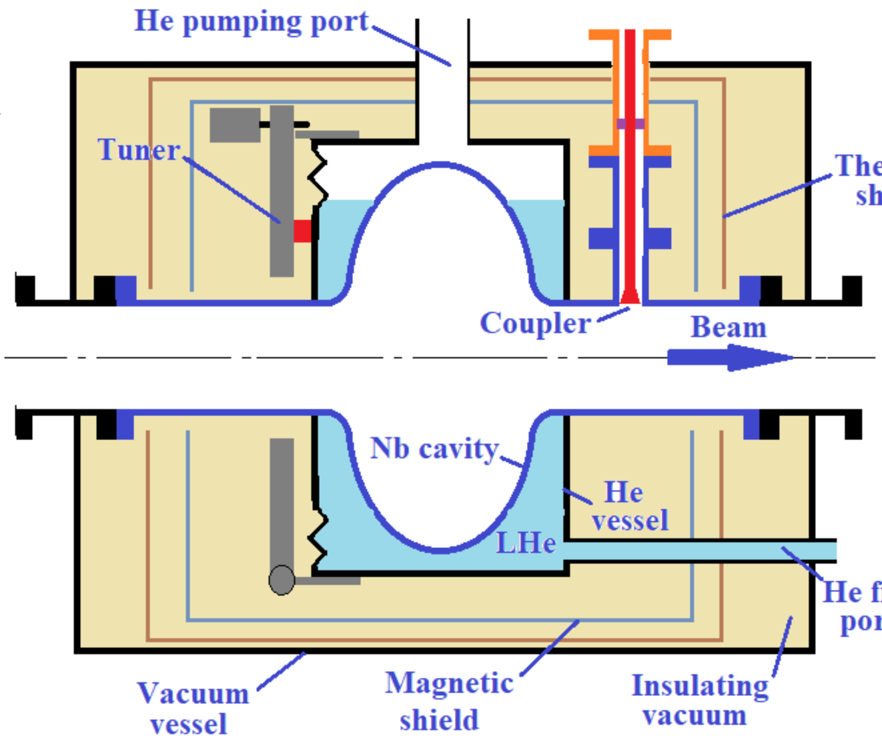

SRF cavity needs:

- Liquid He bath (2K);
- Coarse and fine tuners
- Magnetic shield
- Thermal insulation
- Insulating vacuum
- Cryo plant for liquid He supply

Why SRF?

Refrigeration efficiency (W_{grid}/W_{cryo}):

- Refrigerator's Coefficients of Performance (COP):

$$COP_{real}=1/(\ K * \eta\ CARNOT)$$

$$\eta\ CARNOT = T/(300 - T)$$

- Refrigerator's Coefficients of Performance (COP) for different temperatures:

Refrigeration Temperature	Carnot 1/η IDEAL WORLD	XFEL-Spec REAL WORLD	% Carnot
2 K	149	870	17
5 K	79	220	36
40 K	7	20	33

$$P_{AC} = \sum_T COP_T \times (P_{dynamic} + P_{static})_T$$

In many cases SRF is more efficient than normal conducting RF!

- **Low and medium beam loading**
- **CW and long-pulse operation**

Why SRF?

Thus, SC provides the following benefits for electron, ion and proton linacs:

1. Power consumption is much less
- operating cost savings, better conversion of AC power to beam power
- less RF power sources
2. CW operation at higher gradient possible
- shorter building, capital cost saving
- need fewer cavities for high DF or CW operation
- less beam disruption
3. Freedom to adapt better design for specific accelerator requirements
- large cavity aperture size
- less beam loss, therefore less activation
- HOMs are removed more easily, therefore better beam quality

Why SRF?

"Practical" gradient limitations for SC cavities:

- Surface magnetic field ~ 200 mT (absolute limit?) – "hard" limit
- Field emission, X-ray, starts at ~ 40 MeV/m surface field – "soft" limit
- Thermal breakdown (limits max surface field for f>2GHz for typical thickness of material, can be relaxed for thinner niobium) - "hard" limit

SRF allows significantly higher acceleration gradient than RT at high Duty Factor and CW!

Why SRF?

Different mechanisms limiting acceleration gradient:

Room Temperature:

•Vacuum *Breakdown;*

•*Metal fatigue caused by pulse heating;*

•*Cooling problems.*

Breakdown limit:

$$E_a \cdot t_p^{1/6} = const$$

E_a~ 20 MV/m (E_{pk}~40 MV/m) @ 1ms or

E_a~ 7 MV/m (E_{pk}~14 MV/m) @ 1sec (CW)

Superconducting:

- Breakdown usually is not considered for SC cavity;
- Thermal breakdown (quench) – for >2 GHz

Why SRF?

Achieved Limit of SRF electric field

- No known theoretical limit
- 1990: Peak surface field ~130 MV/m in CW and 210 MV/m in 1ms pulse.

J.Delayen, K.Shepard,"Test a SC rf quadrupole device", Appl.Phys.Lett,57 (1990)

- 2007: Re-entrant cavity: E_{acc}= 59 MV/m (E_{pk}=125 MV/m,B_{pk}=206.5mT).

(R.L. Geng et. al., PAC07_WEPMS006) – World record in accelerating gradient

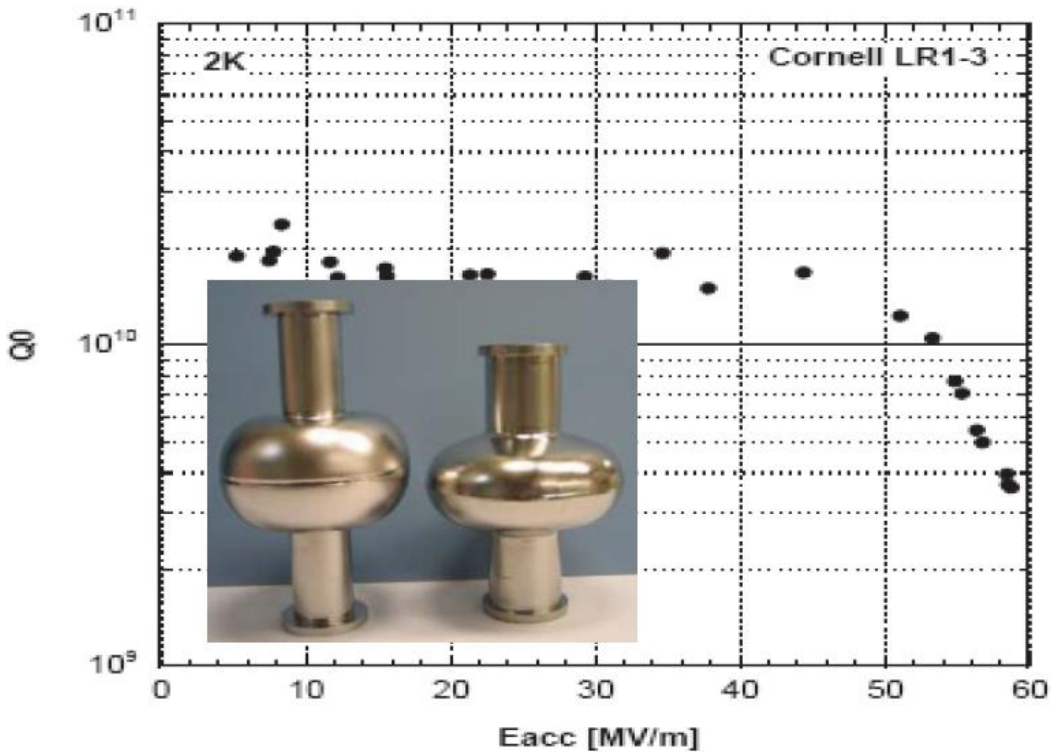

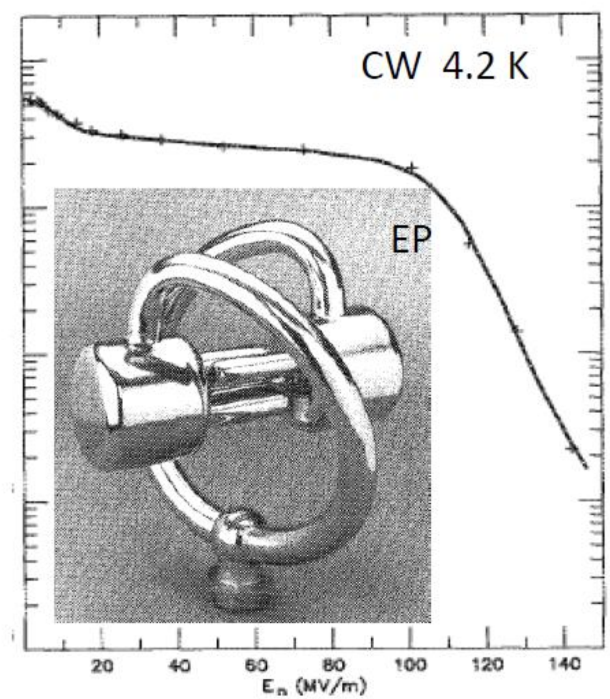

Why SRF?

Introducing Q_0 *vs.* E_{acc} plot:

Typical ILC-prepared TESLA cavity at T = 2 K (state of the art until recent breakthroughs)

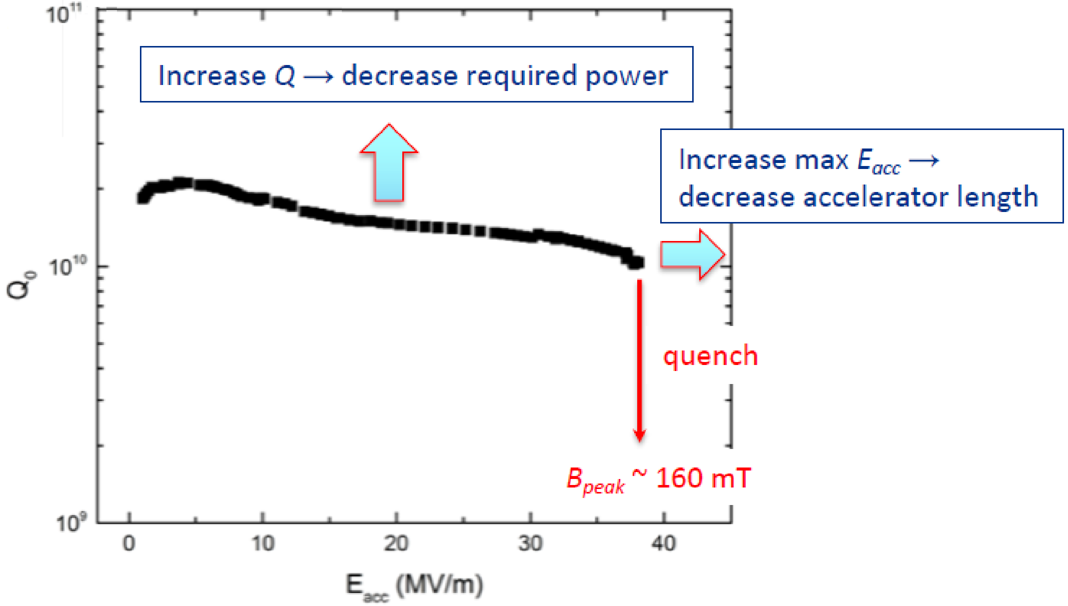

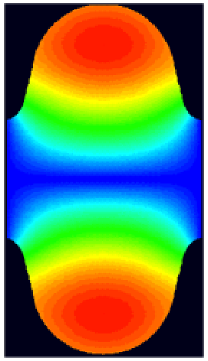

Surface magnetic field *B*

- It is customary to represent performance of an SRF cavity using Q_0 *vs.* E_{acc} *or* $Q_0(E_{acc})$ plot.
- Peak surface electric and magnetic fields in the cavity are proportional to E_{acc}. Sometimes Q_0 is plotted *vs.* peak fields.

Why SRF?

SC cavity performance limitations

- **Ideal performance: Q_0 is constant until the maximal surface magnetic field is reached:**

→ fundamental limitation, limits accelerating gradient to ~60 MV/m for typical Nb elliptical cavity shapes.

- **Why is $Q_0(E_{acc})$ different in real life?**

Here are some limitations that historically plagued the SRF cavity performance:

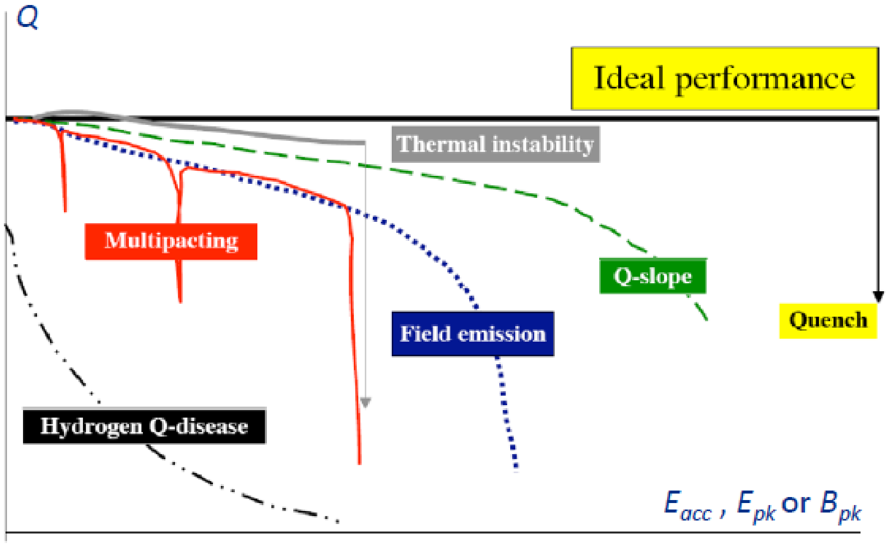

- High surface electric field → field emission → can be cured by applying proper preparation techniques: clean room (particulate-free) assembly, high-pressure DI water rinsing (HPR), mechanical polishing of the inner cavity surface.
- Thermal quench → use of high-purity material (RRR) to improve thermal conductivity*, material quality control to avoid mechanically damaged surfaces, particulate free assembly.
- Multipacting → use of elliptical cell shapes.

Q-disease due to lossy niobium hydrides → perform acid etch at $T < 15$°C, rapid cooldown, degassing at 600 – 800°C.

***Wiedemann–Franz law** states that the ratio of the electronic contribution of the thermal conductivity (κ) to the electrical conductivity (σ) of a metal is proportional to the temperature (T), or $\kappa = \sigma L T$, L is Lorentz number.

Why SRF?

$Q_0(E_{acc})$ with numbers

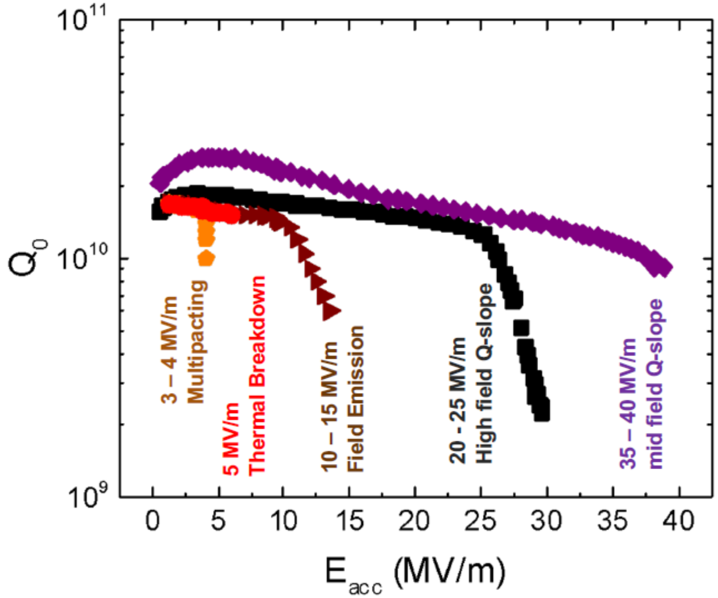

Q slopes

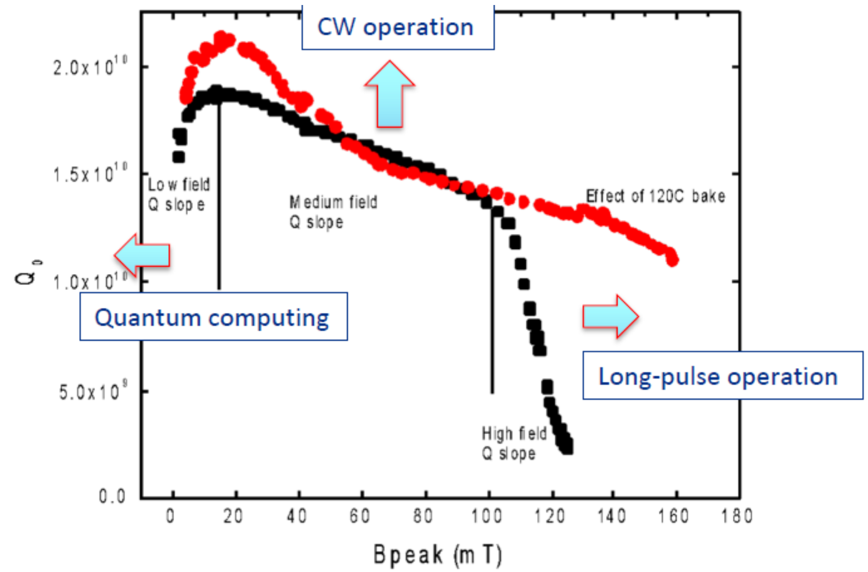

Three parts of the curve limiting performance of different applications:

1. Low field *Q* slope → SRF for quantum computing: need as high *Q* as possible to increase qubit coherence time;
2. Medium field *Q* slope → CW operation: cryogenics vs. linac cost optimization determines operating gradient (15-20 MV/m, LCLS-II);
3. High field *Q* slope → Long-pulse operation tends to favor the highest reliably achievable gradient (23.6 MV/m for XFEL, 31.5 MV/m for ILC)

Why SRF?

Standard SRF cavity surface treatments

- **E**lectron-**B**eam **W**elding - **EBW**
- **B**uffered **C**hemical **P**olishing –**BCP**: $HNO_3+HF+H_3PO_4$
  - H_3PO_4 (phosphoric acid) is necessary to stabilize (buffer) the etching reaction between Nb and HNO_3(nitric acid) +HF (hydrofluoric acid), which is exothermic and rapid.
  - The mixture is used for Nb cavities contains HF(48%), HNO_3 (65%), H_3PO_4(98%) in proportion 1:1:X, X=1-4.
  - Still in use for low-frequency, medium gradient cavities;
- **E**lectro-**P**olishing –**EP**: H_2SO_4+HF+ 10-12V→ smooth surface, lower surface fields, lower FE, higher E_{acc} and Q_0.
  - A cathode made of pure Al and a Nb cavity as an anode in mixture of sulfuric acid H_2SO_4 (93%) and hydrofluoric acid HF (50%) at 10:1 volume ratio.
  - Nb is oxidized by sulfuric acid to nioboum-pentoxide, which is dissolves simultaneously by hydrofluoric acid.
  - Used for high-gradient cavities in pulsed regime and for medium-gradient cavities in CW.
- High-Temperature Treatment
  - 800C -900C backing in vacuum is used to relieve the stresses, remove defects and dislocations and degas of hydrogen.
- **H**igh-**P**ressure **R**insing (HPR)
  - 100 bar rinsing before assembly in a clean room

Why SRF?

BCP processing for a 325 MHz spoke cavity.

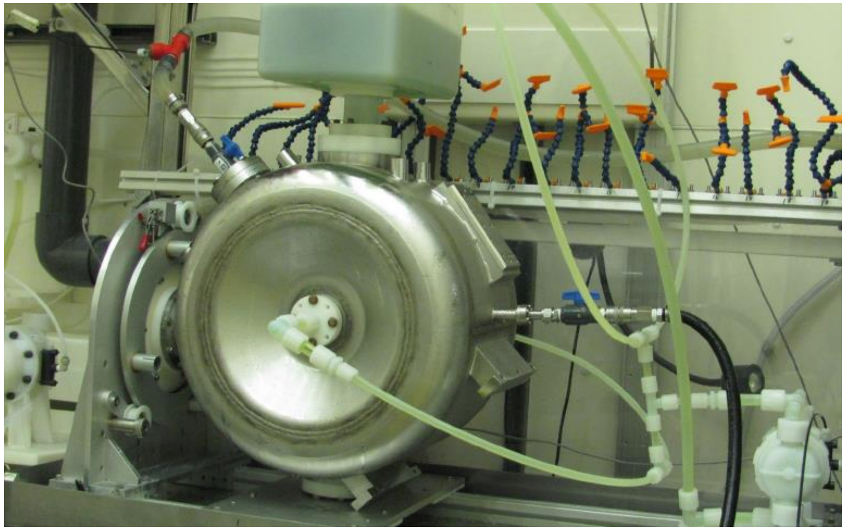

EP processing of 650 MHz elliptical cavity

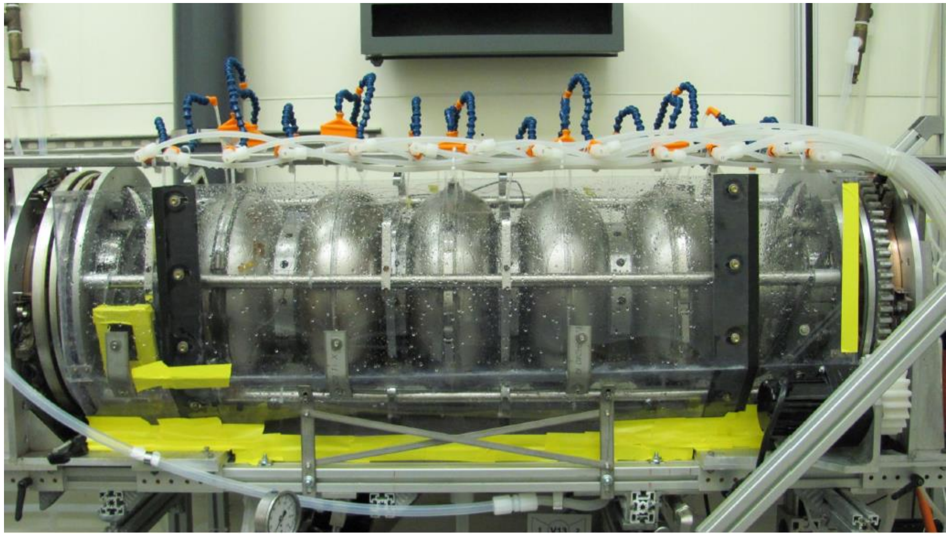

Why SRF?

- Q_0 Improvement:
  - -Improvement of cavity processing recipes;
  - -High Q_0 preservation in CM.
- The goal is to achieve Q_0 >2.5e10- 4e10 in CM

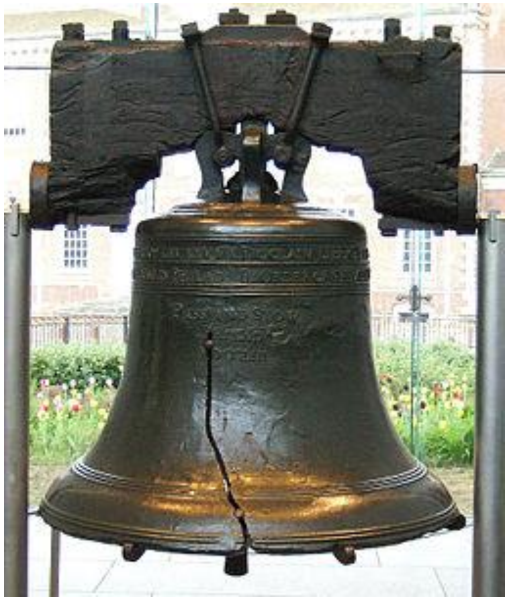

Recent breakthrough in Q_0 increase: N-doping.

- "Standard" XFEL technology provides ~1.4e10@2K, 20-23 MeV/m (CM);
- N-doping: discovered in the frame of R&D on the Project-X SC CW linac (A. Grassellino).

Cavity Treatment:

- Bulk EP
- 800 C anneal for 3 hours in vacuum
- 2 minutes @ 800C nitrogen diffusion
- 800 C for 6 minutes in vacuum
- Vacuum cooling
- 5 microns EP

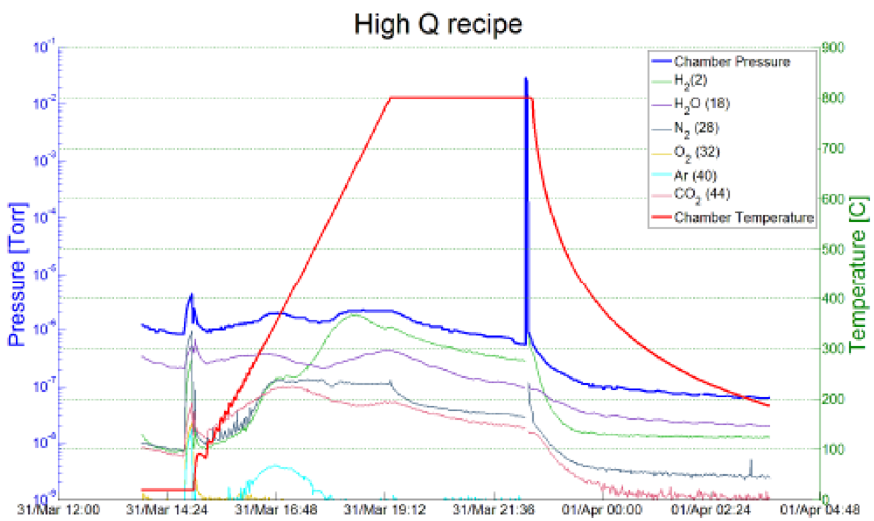

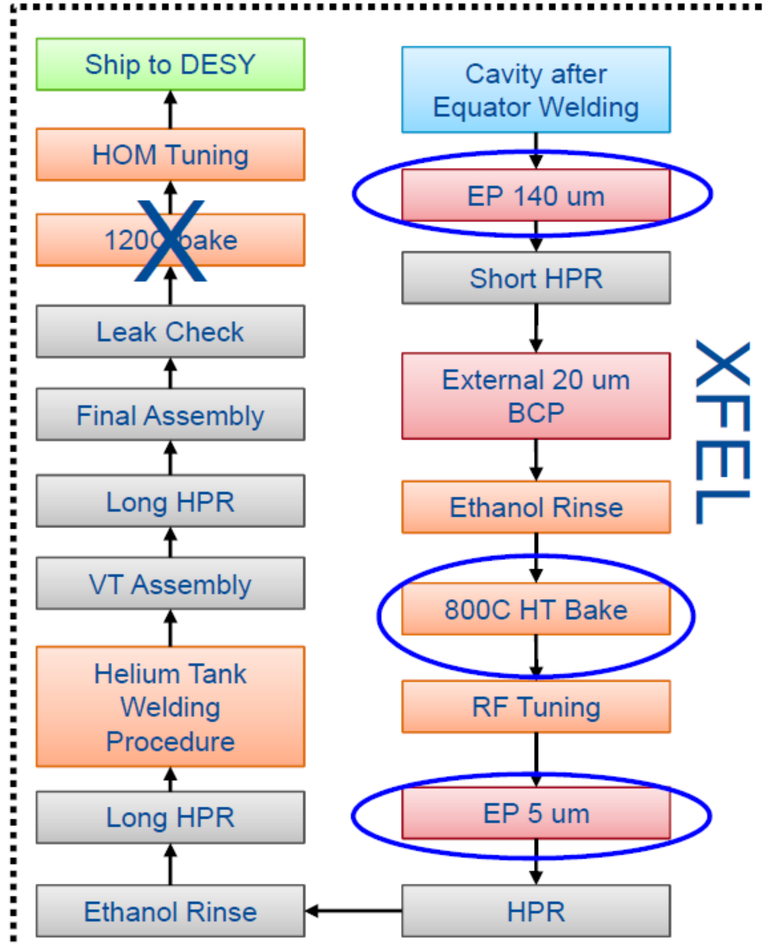

A. Grassellino, N-doping: progress in development and understanding, SRF15

N-doping

Origin of the anti-Q-slope for N-doping

$$R_S(2\ K) = \boxed{R_{BCS}\ (2\ K)} + R_0 + R_{fl}$$

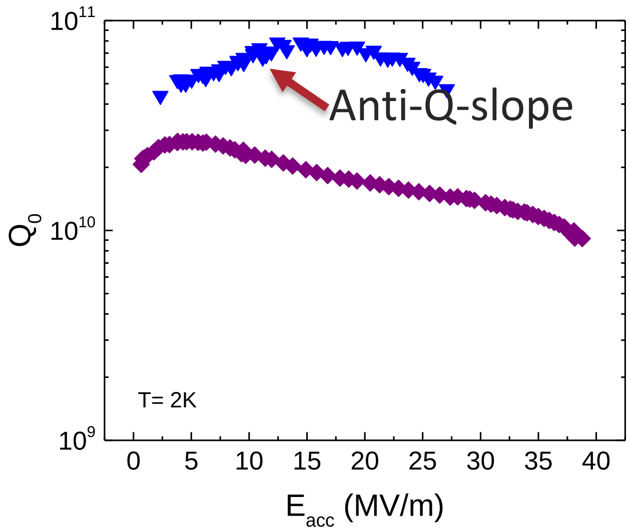

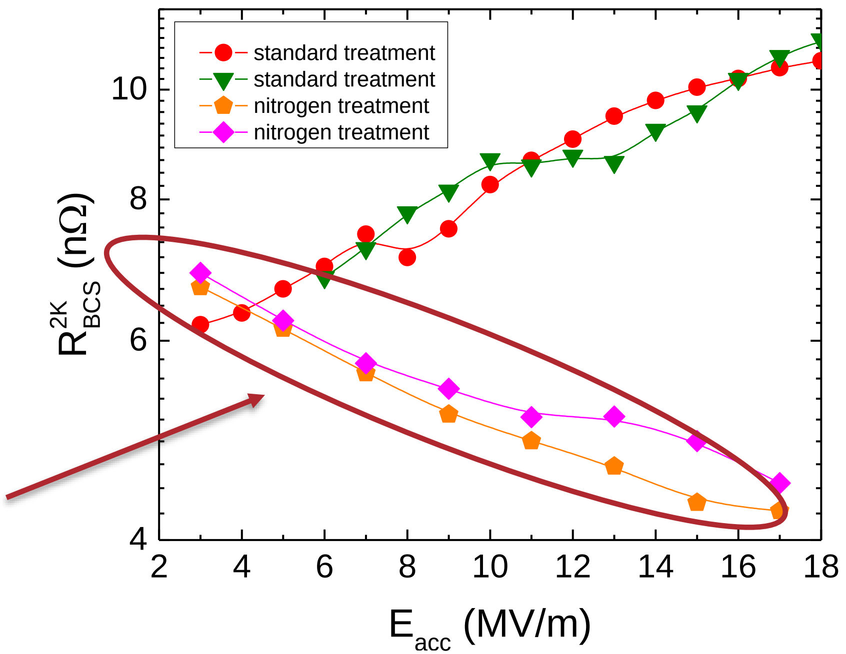

Anti-Q-slope emerges from the BCS surface resistance <u>decreasing</u> with field

A. Grassellino et al, Supercond. Sci. Technol. **26** 102001 (2013) - Rapid Communications
A. Romanenko and A. Grassellino, Appl. Phys. Lett. **102**, 252603 (2013)

M. Martinello, M. Checchin

N-doping:

- Provides Q_0 2.5-3 times higher than "standard" processing.
- Trade-off:
  - Lower acceleration gradient, 20-22 MeV/m – not an issue for ion and proton linacs;
  - Higher sensitivity to the residual magnetic field.
- Remedy:
  - Magnetic hygiene and shielding improvement
  - Fast cooldown

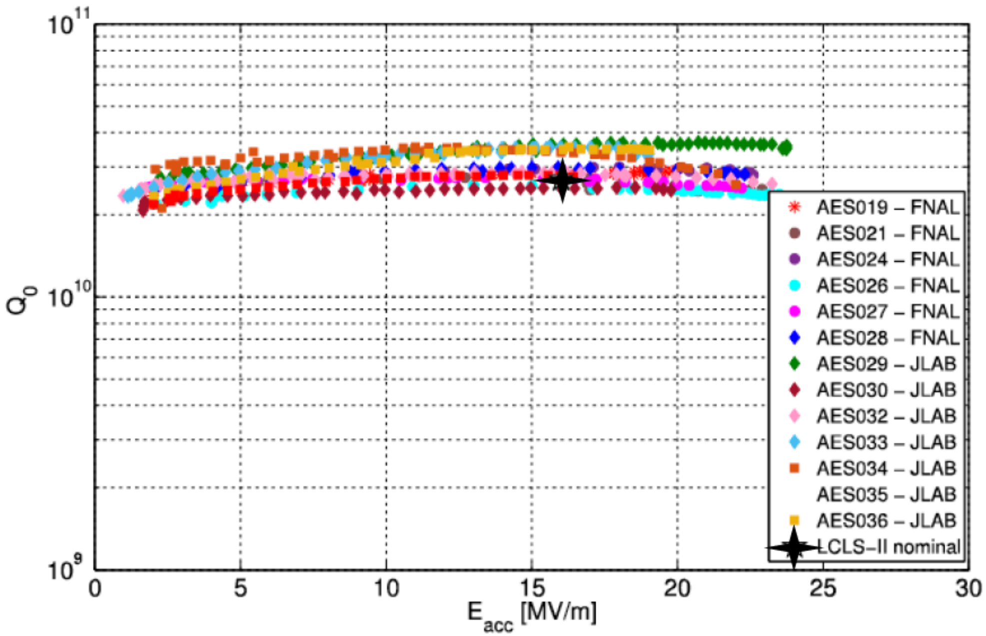

VTS test results of dressed prototype cavities

A. Grassellino, N-doping: progress in development and understanding, SRF15

Fast cooldown

- $Q_0=G/R_s$; R_s=10 nOhm for Q_0=2.7e10

  $R_s=R_0+R_{BCS}+R_{TF}$,

  $R_{TF}=s*\eta*B_{res}$, s is sensitivity to residual magnetic field B_{res}, η is flux expulsion efficiency.

  η is material-dependent!
- For pCM Nb (Wah Chang):

  R_{BCS}=4.5 nOhm, R_0=1-2 nOhm, $R_{TF}\approx$1 Ohm for 5mG → Q_0=3.5e10
- For production material:

  Change heat treatment temperature from 800 C to 900 C+ deeper EP (S. Posen):

  R_{BCS}=4.5 nOhm, $R_0 \approx$ 2 nOhm, $R_{TF} \approx$2 Ohm for $B_{res} \approx$ 5mG → Q_0 >3e10

Dressed N_2 doped 9 cell Sensitivity Test at 2K

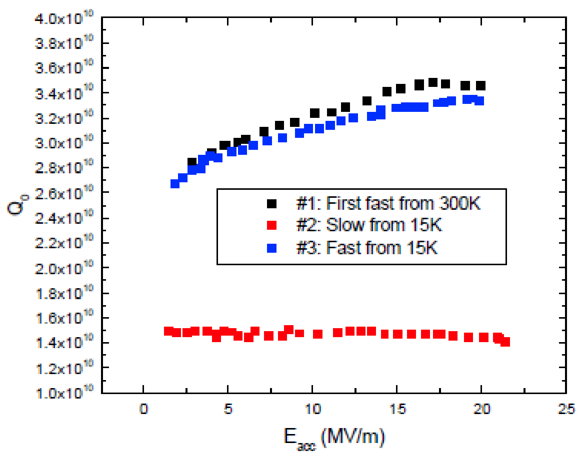

"Fast": 2 – 3 K/minute ,"slow": < 0.5 K/minute

A. Grassellino, N-doping: progress in development and understanding, SRF15

Impact of Modified LCLS-II Recipe on Q_0

Cavities 17, 18, 19: modified recipe - 900 C degas, ~200 µm EP, 2min/6min N doping at 800 C

Cavities 03…16: First production tests at Fermilab, baseline LCLS-II recipe - 800 C degas, ~130 µm EP, 2min/6min N doping at 800 C

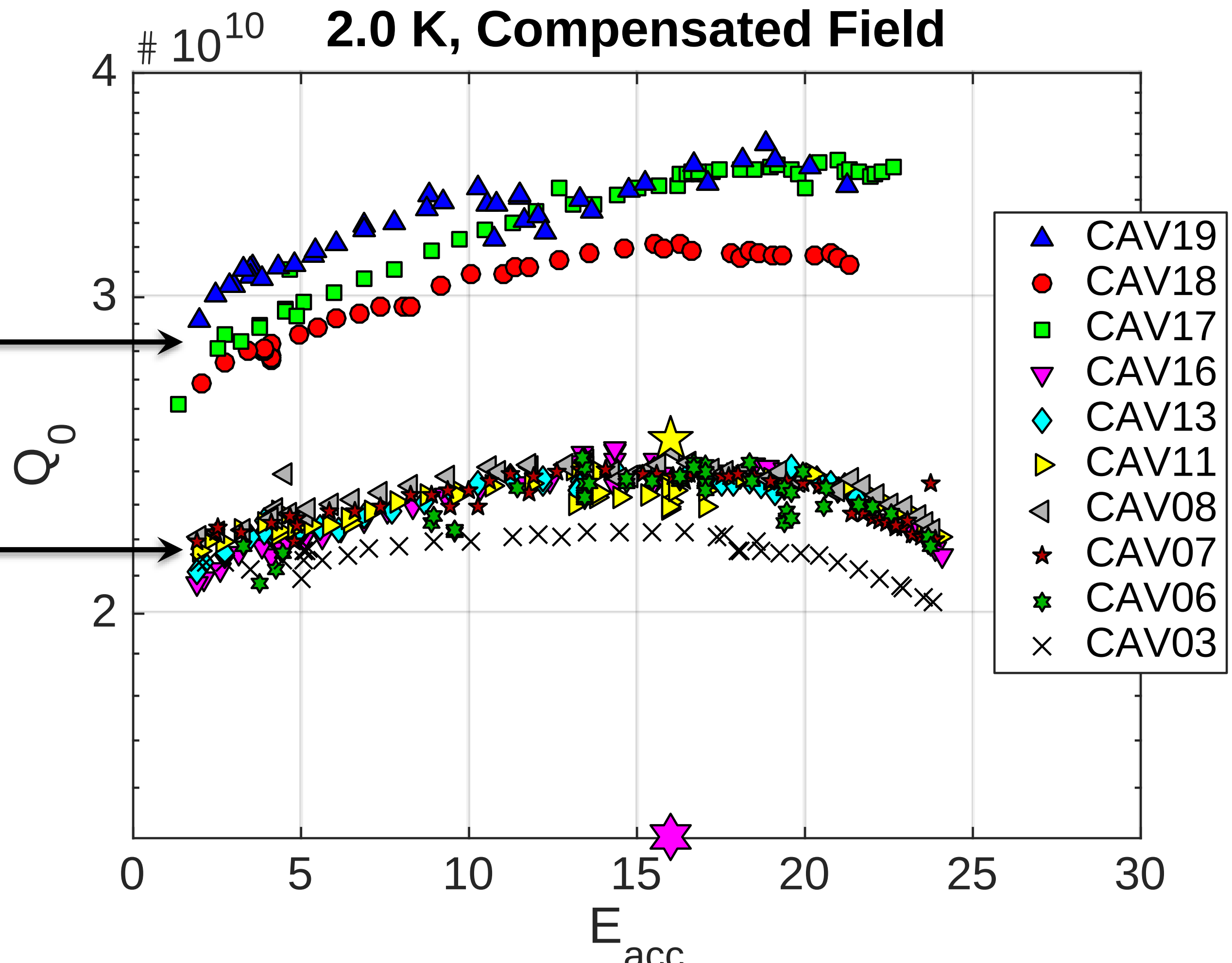

<u>Studies leading to modified recipe:</u>

S. Posen, M. Checchin, A. C. Crawford, A. Grassellino, M. Martinello, O. S. Melnychuk, A. Romanenko, D. A. Sergatskov and Y. Trenikhina, *Efficient expulsion of magnetic flux in superconducting radiofrequency cavities for high Q_0 applications*, J. Appl. Phys. **119**, 213903 (2016), dx.doi.org/10.1063/1.4953087 .

A. Romanenko, A. Grassellino, A. C. Crawford, D. A. Sergatskov and O. Melnychuk, *Ultra-high quality factors in superconducting niobium cavities in ambient magnetic fields up to 190 mG*, Appl. Phys. Lett. **105**, 234103 (2014); http://dx.doi.org/10.1063/1.4903808 .

A. Grassellino, A. Romanenko, S Posen, Y. Trenikhina, O. Melnychuk, D.A. Sergatskov, M. Merio, N-doping: progress in development and understanding, Proceedings of SRF15, http://srf2015proc.triumf.ca/prepress/papers/moba06.pdf .

Ambient Magnetic Field Management Methods

- 2-layer passive magnetic shielding
  - Manufactured from Cryoperm 10
- Strict magnetic hygiene program
  - Material choices
  - Inspection & demagnetization of components near cavities
  - Demagnetization of vacuum vessel
  - Demagnetization of assembled cryomodule / vessel
- Active longitudinal magnetic field cancellation

Magnetic field diagnostics:

- 4 cavities instrumented with fluxgates inside helium vessel (2 fluxgates/cavity)
- 5 fluxgates outside the cavities mounted between the two layers of magnetic shields

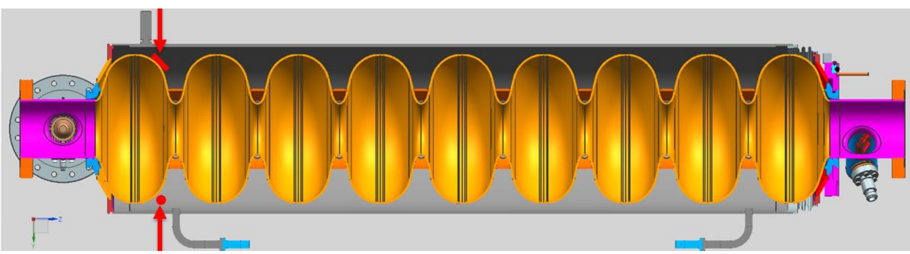

Fluxgates monitored during cryomodule assembly

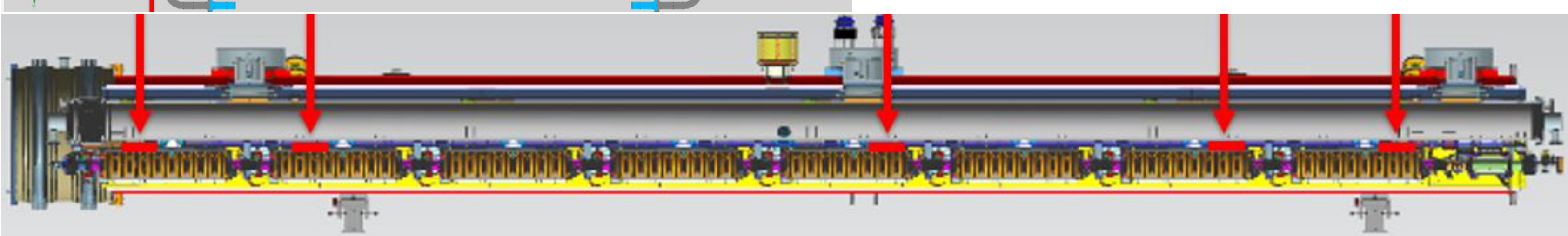

A. Crawford, arXiv:1507.06582v1, July 2015; S. Chandrasekaran, TTC Meeting, Saclay 2016

Ambient Magnetic Field Management Methods

Helmholtz coils wound onto vessel directly

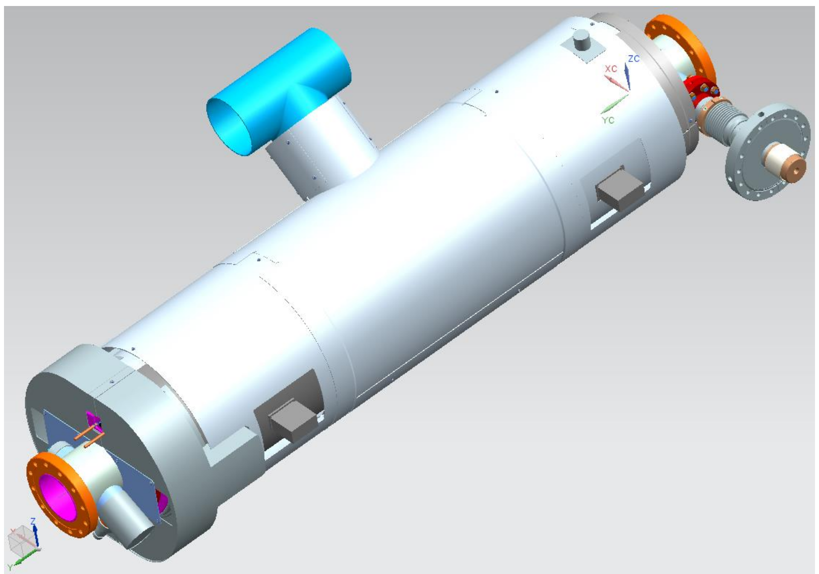

2-layer magnetic shields
manufactured from Cryoperm 10

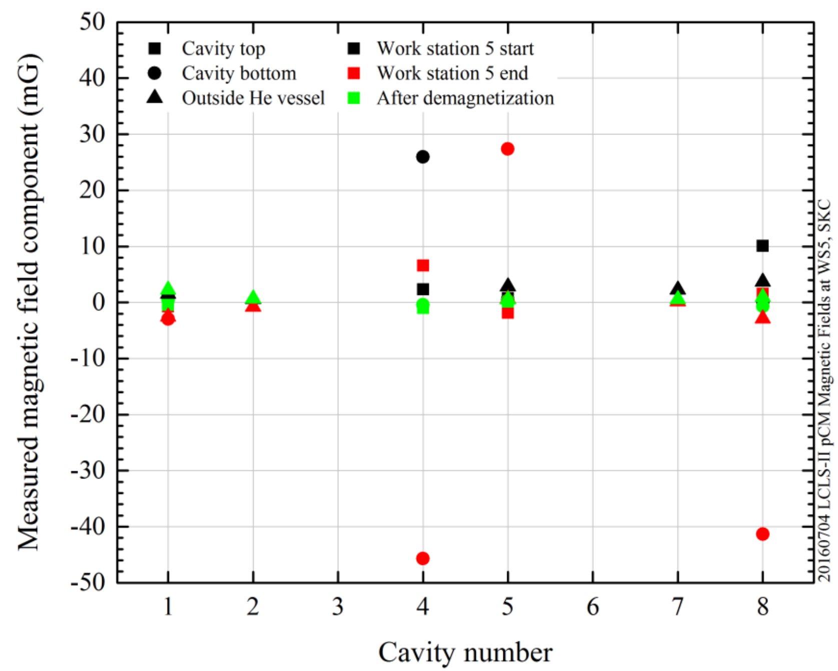

S. Chandrasekaran, Linac 2016, TUPLR027

Prototype Cryomodule Latest Preliminary Results

- Cryomodule remnant field ≈ 1 mG
- Fast cool down in a cryomodule demonstrated
- Q0 ≈ 2.7e10 in a CW cryomodule

	VTS		pCM after RF_Conditioning			
Cavity	**Max Gradient [MV/m]**	**Q0 @16MV/m**	**Max Gradient*** [MV/m]**	**Usable Gradient* [MV/m]**	**FE onset [MV/m]**	**Q0 @16MV/m 2K** extrapolated**
TB9AES021	23	3.1E+10	19.6	18.2	14.6	2.6E+10
TB9AES019	19.5	2.8E+10	19	18.8	15.6	2.6E+10
TB9AES026	21.4	2.6E+10	17.3	17.2	17.4	2.7E+10
TB9AES024	22.4	3.0E+10	21	20.5	21	2.5E+10
TB9AES028	28.4	2.8E+10	14.9	14.2	13.9	2.4E+10
TB9AES016	18	2.8E+10	17.1	16.9	14.5	2.9E+10
TB9AES022	21.2	2.8E+10	20	19.4	12.7	3.2E+10
TB9AES027	22.5	2.8E+10	20	17.5	20	2.5E+10
Average	**22.1**	**2.8E+10**	**18.6**	**17.8**	**16.2**	**2.7E+10**
Total Voltage	**183.1 MV**		**154.6**	**148.1**		

*Usable Gradient: demonstrated to stably run CW, FE < 50 mR/h, no dark current

**Fast cooldown from 45K, >40 g/sec, extrapolated from 2.11K

G. Wu, FNAL SRF Department meeting, 24 October 2016, https://indico.fnal.gov/conferenceDisplay.py?confId=13185

Further Improving cavity performance via surface treatment

- Breakthrough caused by invention of **nitrogen doping** (N-doping) triggered investigations of other surface treatment methods:
  - Mid-T backing and
  - Cold EP & 2-step baking.

New surface treatments

Nitrogen doping

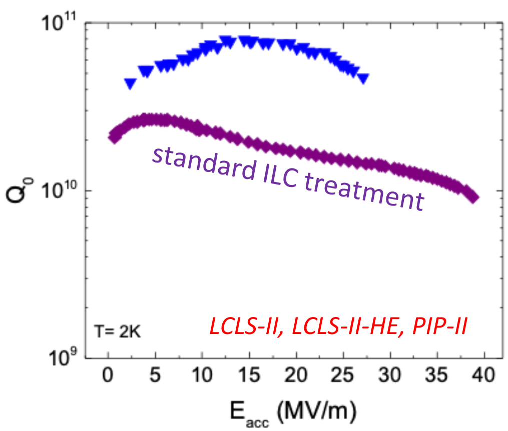

Mid-T baking

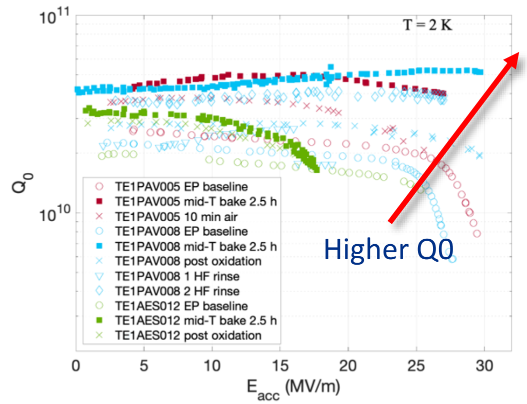

*PIP-II, CEPC, FCC-ee, **ERLC, ReLiC***

Cold EP & 2-step low-temperature baking

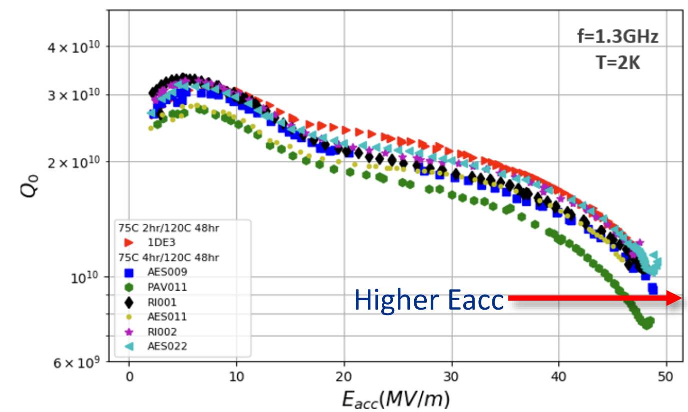

***ILC, HELEN**, 8-GeV linac at FNAL*

- There are active studies to push performance of bulk niobium cavities, improve our understanding of SRF losses and ultimate quench fields via experimental and theoretical investigations
- The ultimate goal is on developing methods for nano-engineering the niobium surface layer and tailoring SRF cavity performance to a specific application

Mid-T baking: Initial results

- Medium temperature baking in vacuum (Mid-T, 300°C to 400°C) was developed to improve cryogenic performance of SRF cavities at medium accelerating gradients (E_{acc} = 20 – 30 MV/m), extending beyond N-doping in E_{acc} while maintaining high Q_0

This is a new, simpler alternative to nitrogen doping

Mid-T baking

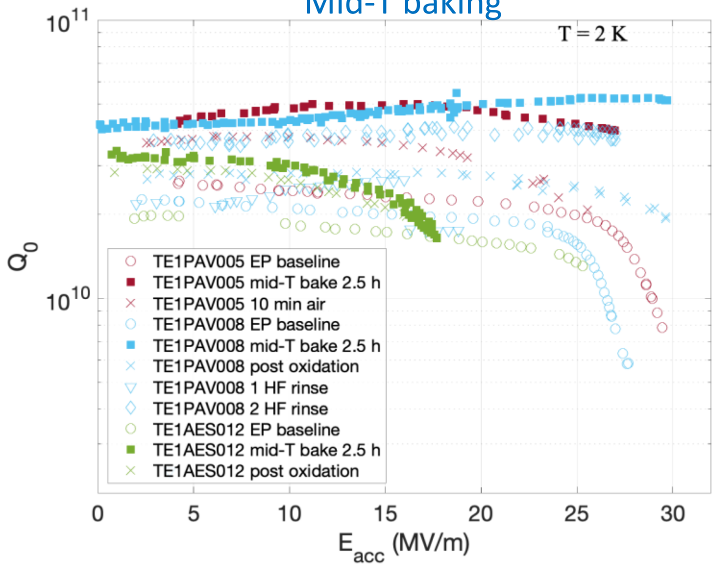

S. Posen et al. *Phys. Rev. Applied* **13**, 014024 (2020)

Note: Our standard "vehicle" for R&D is a single-cell 1.3 GHz elliptical TESLA shape cavity

Mid-T baking at 650 MHz (5-cell cavities)

- After initial R&D efforts at 1.3 GHz, this recipe was successfully tested on the low-beta 650 MHz (LB650) PIP-II cavities and was accepted as a baseline treatment

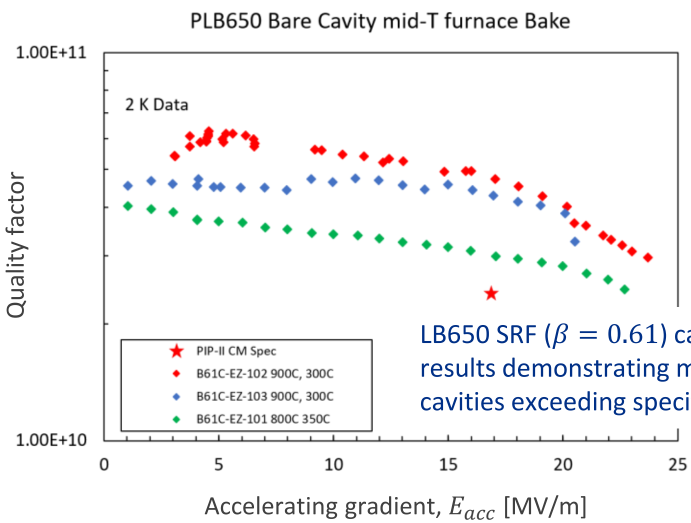

LB650 SRF ($\beta = 0.61$) cavity test results demonstrating mid-T cavities exceeding specifications

Courtesy of Genfa Wu (FNAL)

Note: Need to multiply Q by a factor of 1.4 to compare with TESLA shape cavities

PIP-II LB650 SRF cavity

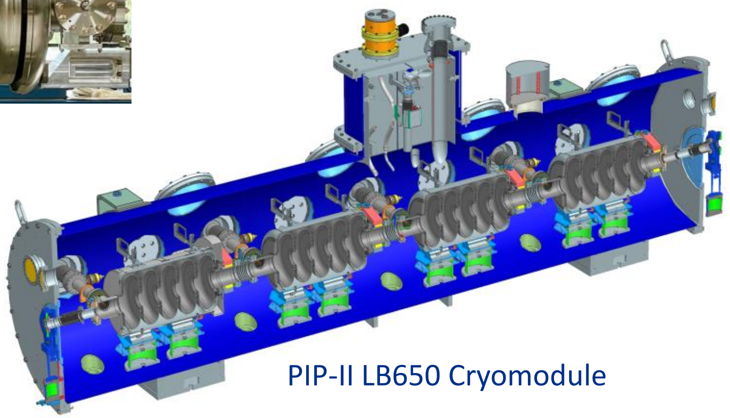

PIP-II LB650 Cryomodule

- Mid-T baking is relevant to ERL-based liner colliders (as well as circular colliders)

Pushing toward 50 MV/m

- Application of a combination of cold electropolishing (EP) and 2-step low-temperature baking to single-cell TESLA cavities demonstrated accelerating gradients ~ 50 MV/m
- The recipe is transferred to 9-cell cavities: average 40.4 MV/m!
- A High-Gradient Cryomodule (HGC) is being prepared at Fermilab for testing

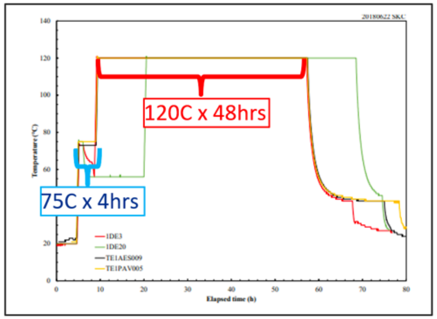

Grassellino et al. https://arxiv.org/abs/1806.09824

2-step low-temperature baking (single-cell cavities)

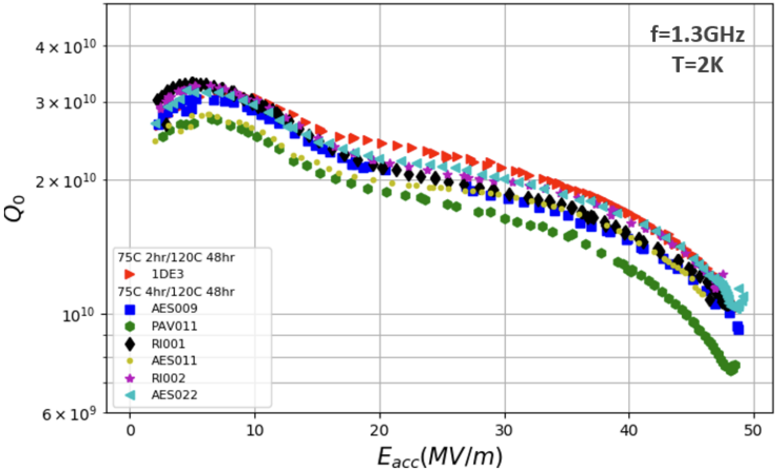

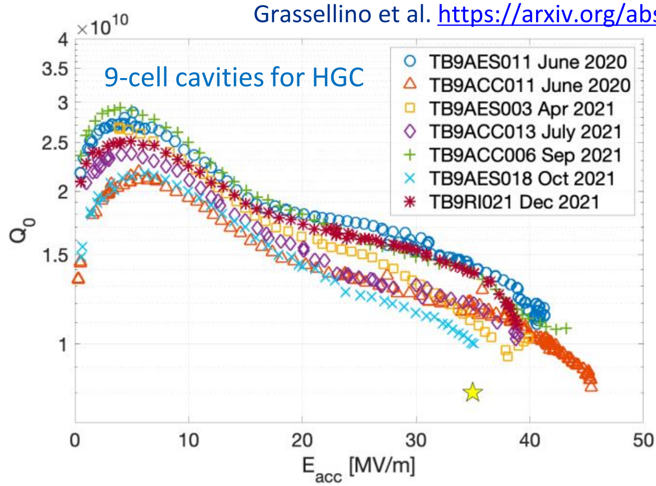

Fermilab

Cold EP or 2-step baking?

- It is not clear yet, whether cold EP, 2-step baking (as opposed to standard low-temperature baking) or a combination of both is responsible for improving accelerating gradient
- Cold EP provides much smoother surface than EP at higher temperatures
- Recently, a 9-cell cavity subjected to cold EP and 120℃ baking reached 46 MV/m
- Systematic studies are under way

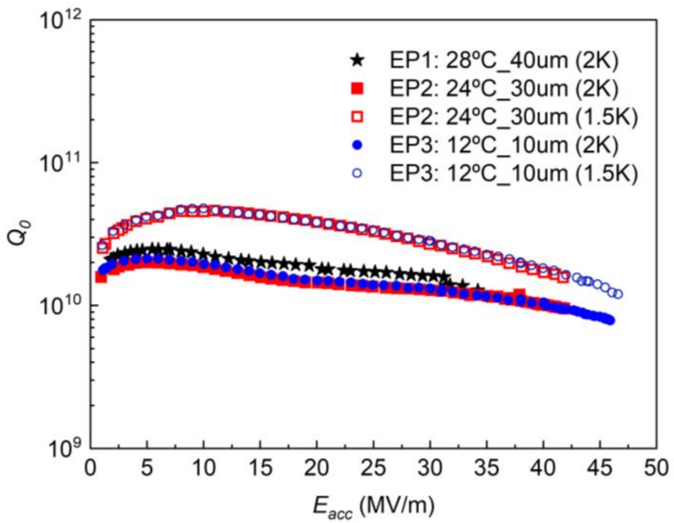

Courtesy of V. Chouhan (FNAL)

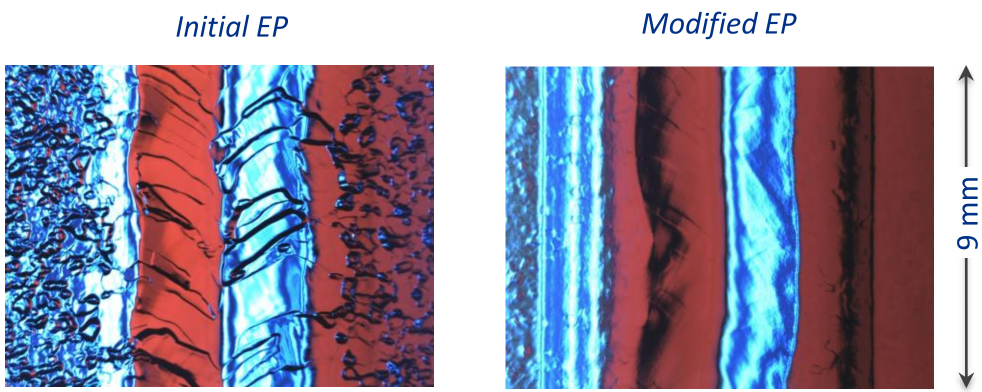

V. Chouhan *et al.*, *Nucl. Instrum. Methods Phys. Res. A* **1051** (2023) 168234

Recent results on single-cell 650 MHz cavities

- Recently, cold EP and 120℃ backing applied to single-cell 650 MHz cavities produced excellent results at IHEP (China)
- Similar performance was demonstrated at Fermilab

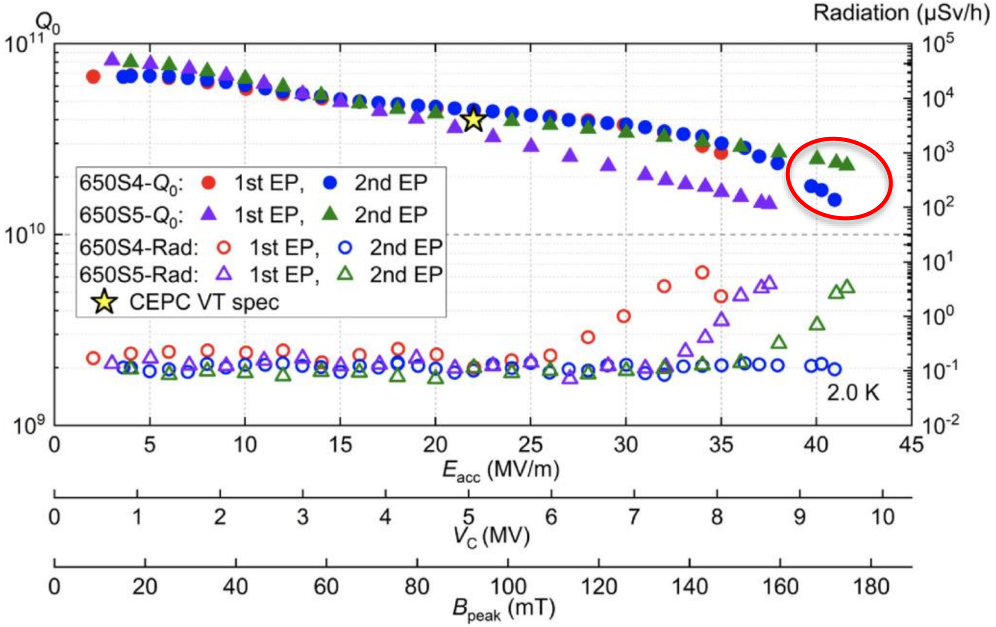

P. Sha et al. *Nucl. Sci. Tech.* (2022) **33**:125

New materials: Nb_3Sn

- High T_c material → low losses at 4 K, a candidate for cryocooler-based applications
- **Potential for high gradients**, ~ 90 MV/m
- So far, the best progress with **vapor diffusion technique**

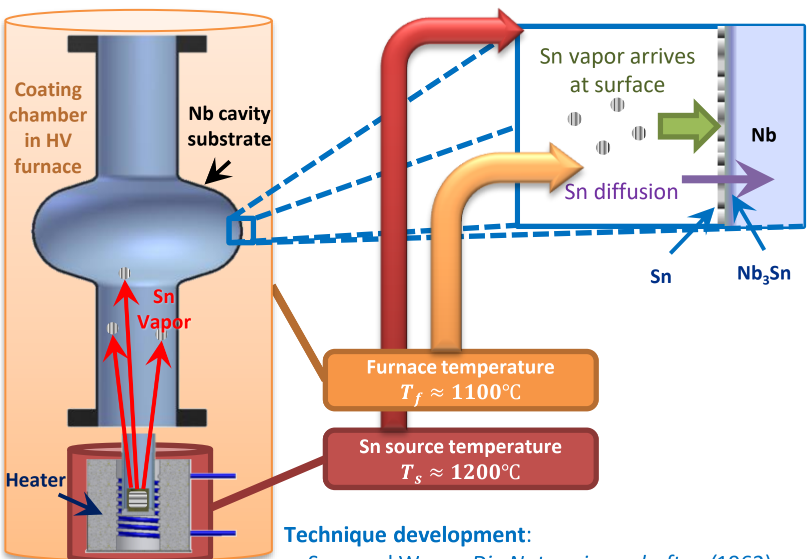

Technique development:
Saur and Wurm, *Die Naturwissenschaften* (1962)
Hillenbrand et al., *IEEE Transactions on Magnetics* (1977)
Peiniger et al., *Proceedings of SRF'88*

- Best performance of a single-cell Nb_3Sn cavity so far is only ~ 24 MV/m

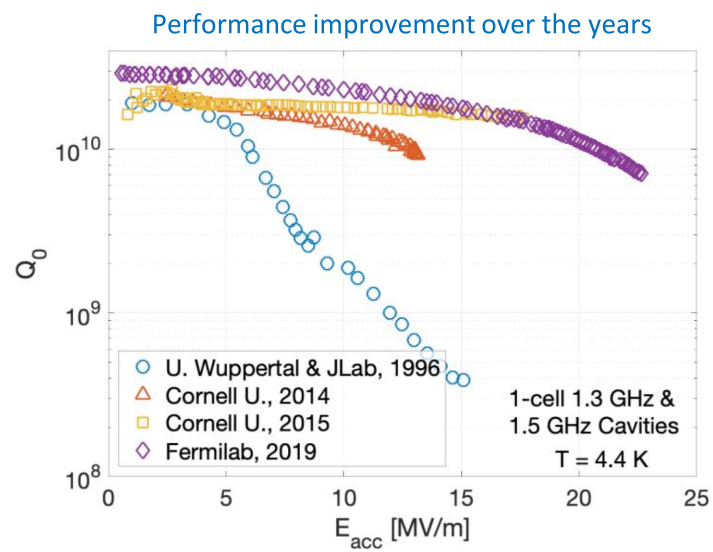

Multi-cell Nb_3Sn cavities

- The best multi-cell cavities reached 15 MV/m

Nb_3Sn-coated 1.3 GHz 9-cell cavities

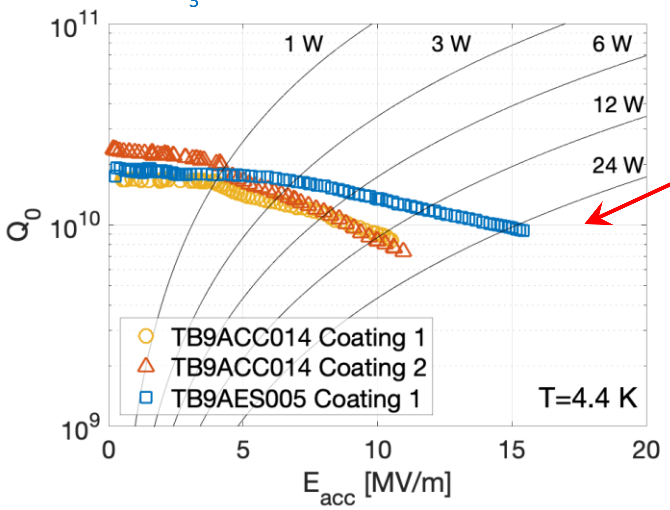

Courtesy of S. Posen (FNAL)

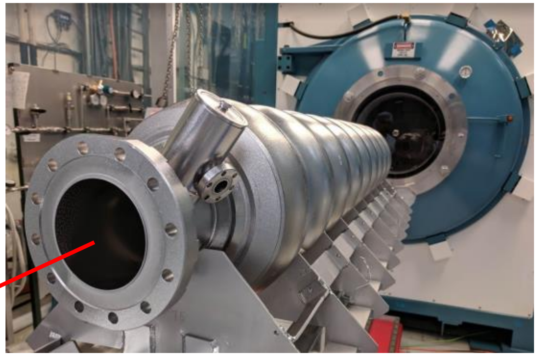

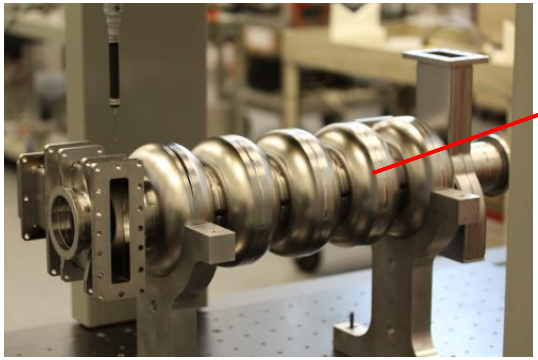

Nb_3Sn-coated 1.5 GHz 5-cell cavities

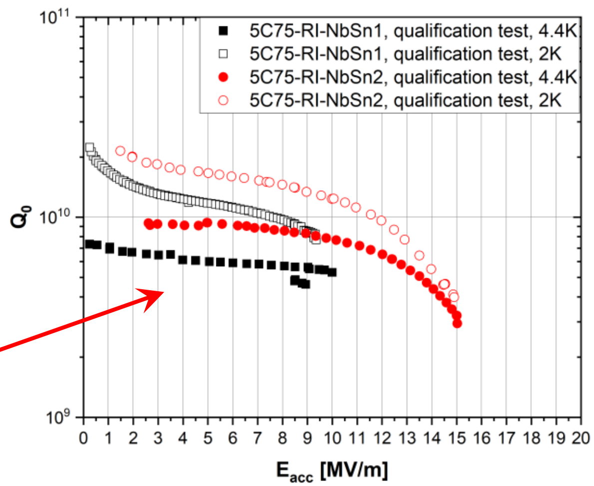

G. Eremeev and U. Pudasaini, presentation at the *TTC meeting,* October 2022

Fermilab

Conduction-cooled cavities

- Conduction cooling of Nb_3Sn SRF cavities via a cryocooler was demonstrated recently
- This is promising for **new compact accelerator applications for industry**

Fermilab

R.C. Dhuley et al, *Supercond. Sci. Technol.* **33,** 06LT01 (2020)

Cornell University

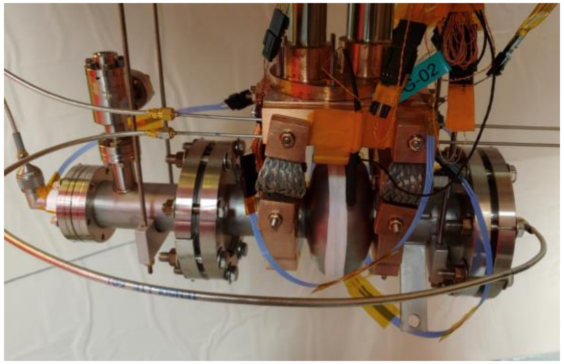

N. Stilin et al, arXiv:2002.11755v1 (2020)

Jefferson Lab

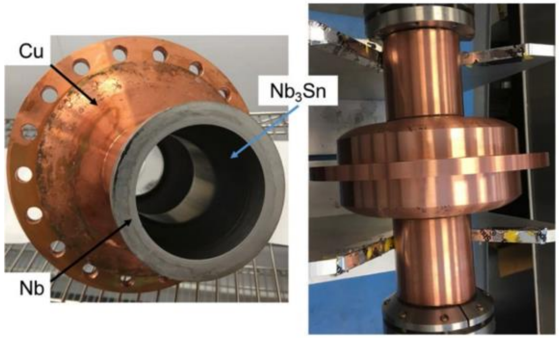

G. Ciovati et al, *Supercond. Sci. Technol.* **33**, 07LT01 (2020)

Multipacting (MP) in SRF cavities

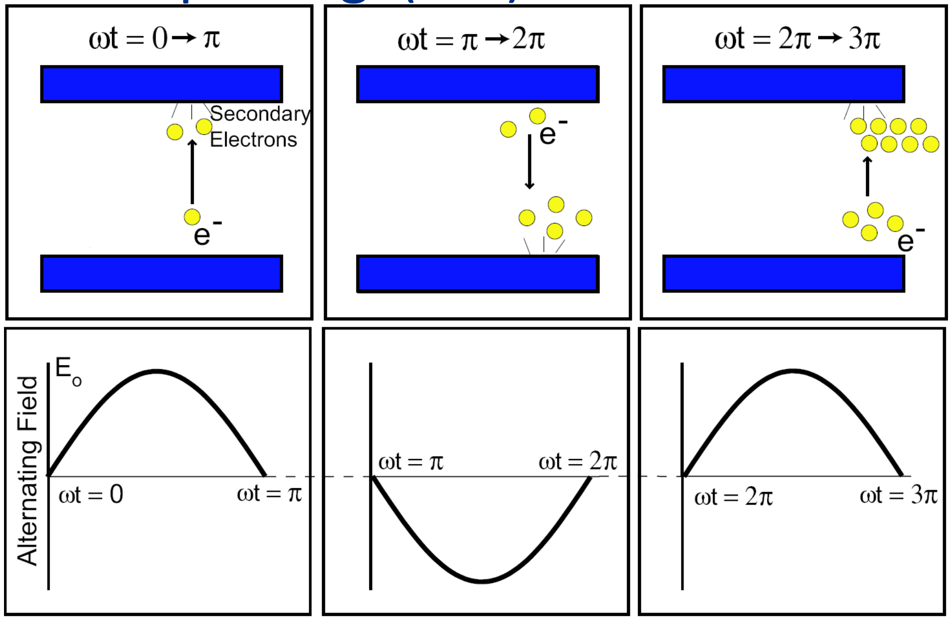

Multipactor discharge with an electric field oscillating between two metal electrodes.

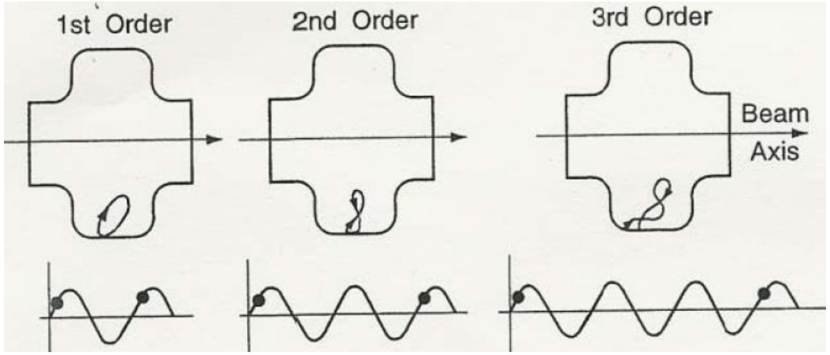

Typical one-point multipactor trajectories for orders 1, 2 and 3.

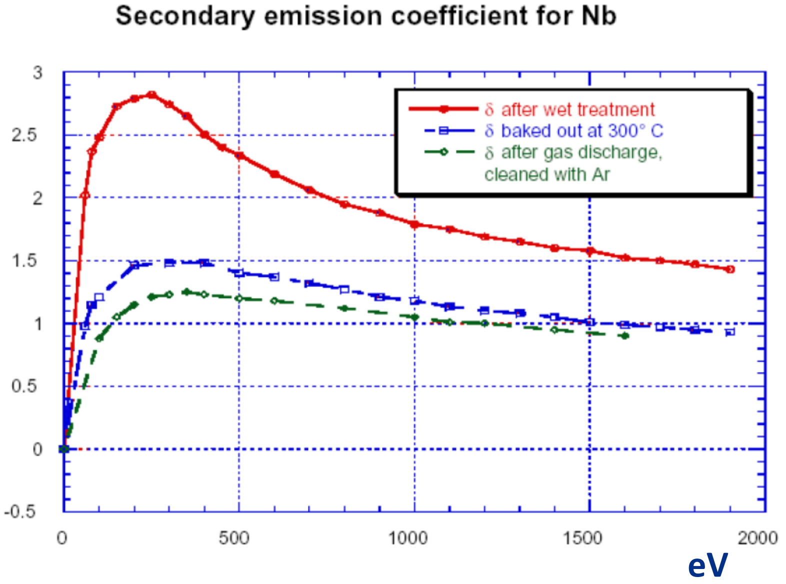

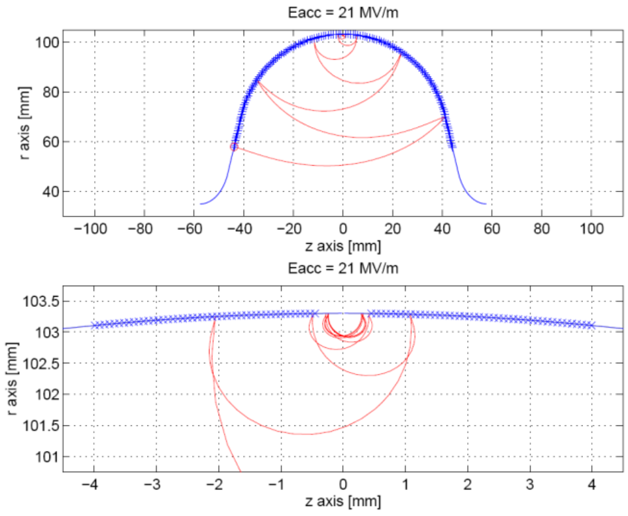

Two point MP in 1.3GHz TESLA cavity. 2D simulations

Fermilab

Multipacting in SRF cavities

SSR1 cavity

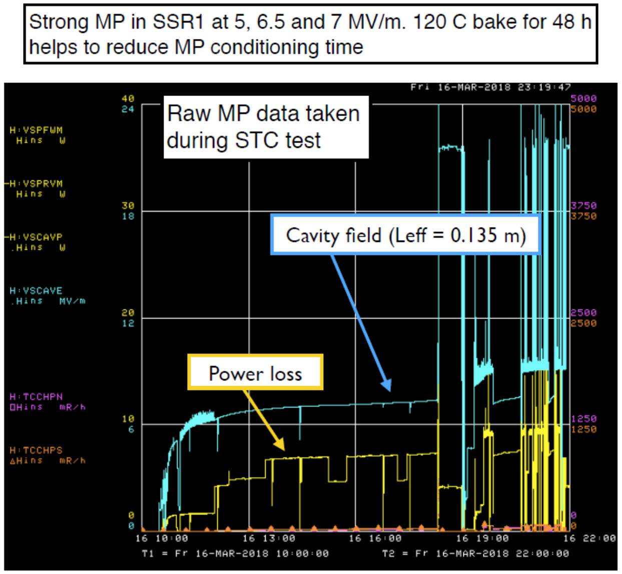

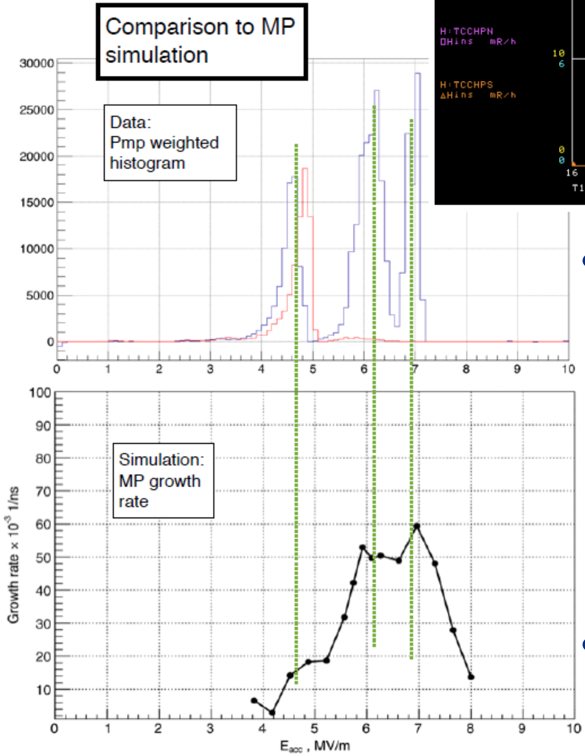

Good agreement between MP conditioning data (Pmp weighted histogram) and MP simulation (growth rate)

- **QWR, HWR and SSR are prone to MP, need up to 10 -15 hours to process;**
- **Elliptical cavities have much better performance.**

3.9 GHz HOM coupler failure due to overheating caused by MP: redesigned to shift MP barriers above operating gradients

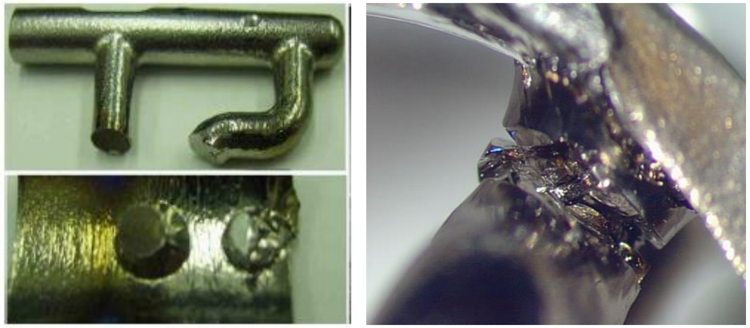

Multipacting in HOM2 at SNS

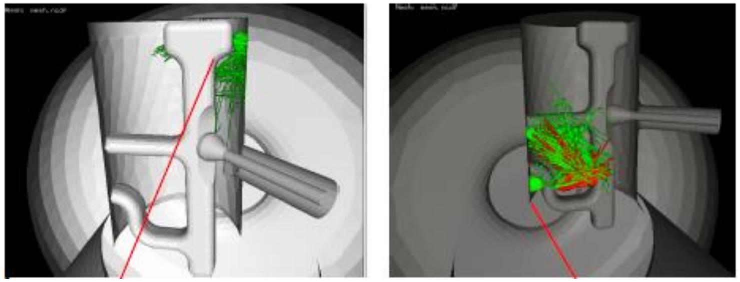

Field emission (FE) and dark currents in SRF cavities

- FE in SRF cavities is originated from *localized sites* on the inner cavity surface.
- The predominant source emitters are microscopic particulates adhering to the inner cavity surface, chemical residuals, and geometrical flaws.
  - Field emitters introduced by the necessary chemical surface processing → post chemistry ultrasonic cleaning and high pressure water rising.
  - Field emitters introduced through the cavity opening ports onto the cavity surface, at a time beyond the completion of final cleaning, from external sources → SRF cavities are assembled in large-sized high-quality Class 10 cleanliness clean rooms into cavity strings; critical assembly steps are done with the opening port facing down; cavity strings are evacuated slowly etc.
- Diagnostics:
  - X-ray monitoring/mapping
  - Temperature monitoring/ mapping
  - Electron detecting
  - Optical imaging:

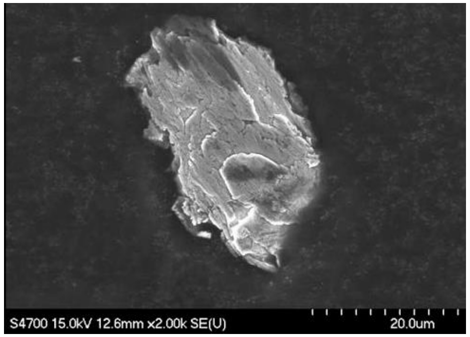

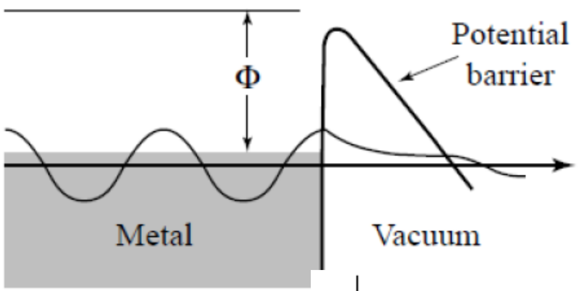

The tunneling current density, $j(E)$

$$J(E) = k\frac{1.54\times10^{-6}(\beta E)^{5/2}}{\Phi}\exp\left(-\frac{6.83\times10^{9}\Phi^{3/2}}{\beta E}\right)$$

j – current density in A/m^2,
E – surface electric field in MV/m,
Φ – work function in eV,
β – field enhancement factor (10-100)
k – effective emitting surface area.

Field enhancement factor β :

For a spherical protrusion in a metal wall β =3

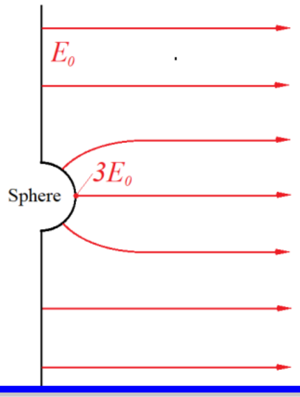

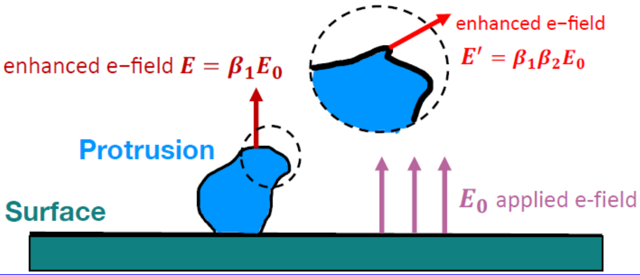

Fermilab

Field emission (FE) and dark currents in SRF cavities

Effect of dark current

- heat and RF loading of the cavity
- production of avalanches of secondary electrons
- accelerating to hundreds of MeV before being kicked out by down stream quadrupoles
- originating electromagnetic cascade showers in the surrounding materials

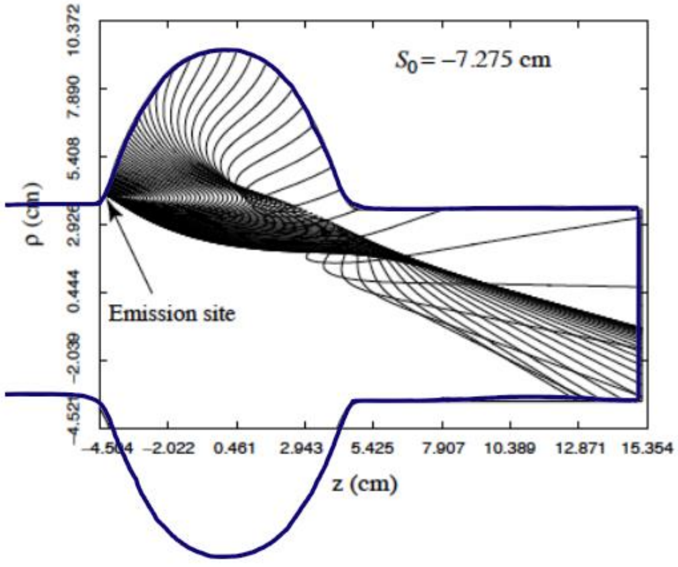

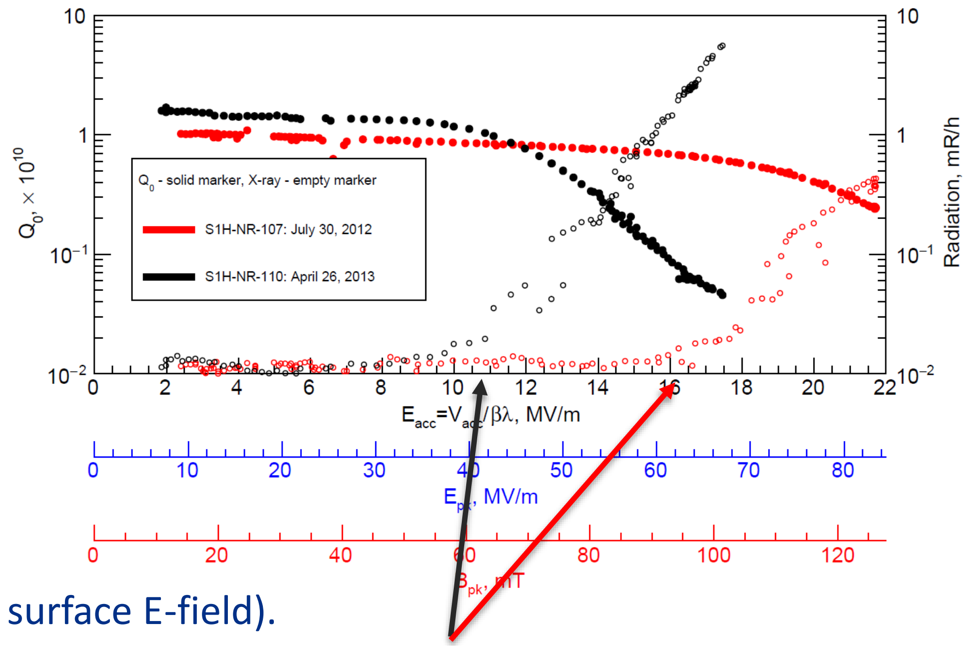

- The emitter is located at the cell entrance (high surface E-field).
- Significant number of FE electrons bend back in the H-field and strike the wall

In situ field emission mitigation via plasma processing

- While procedures of the cryomodule cavity string assembly are being improved continuously (e.g., R&D on using robotic manipulators), field emission (FE) remains a problem
- Plasma processing was first developed at Oak Ridge National Laboratory
- Gas flow of Ne-O mixture (mostly Ne with a few % of O_2) at pressure ~ 75-150 mTorr. Argon is used
- Once plasma is ignited, oxygen reacts with hydrocarbons
- Reaction products (mostly CO, CO_2, H_2O) are pumped out
- Work function increases, reducing FE
- This method was adapted to LCLS-II and LCLS-II-HE and being investigated for other applications including International Linear Collider
- Recently it was demonstrated that plasma processing helps mitigating multipacting as well

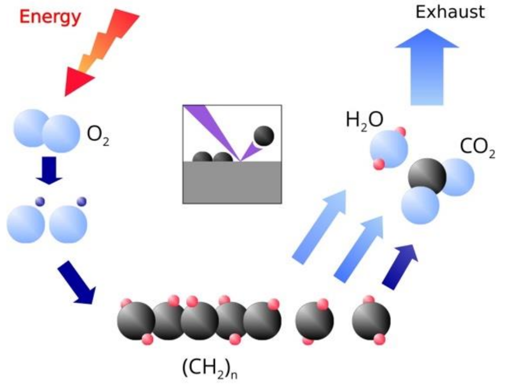

M. Doleans, et al., *Nucl. Instrum. Methods Phys. Res. A* **812**, 50-59 (2016)

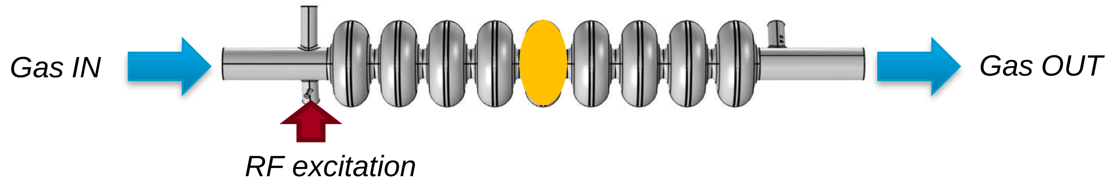

P. Berrutti, et al., *J. Appl. Phys.* **126**, 023302 (2019); B. Giaccone et al., *Phys. Rev. Accel. Beams* **24**, 022002 (2021)

Microphonics and Lorentz Force Detune:

Narrow bandwidth of the cavities caused by low beam loading:

- $Q_{load} = U/(R/Q)/I_{beam}$ - very high for small beam current of few mA, Q_{load} ~1e7-1e8;
- Cavity bandwidth: f/Q_{load} ~tens of Hz.

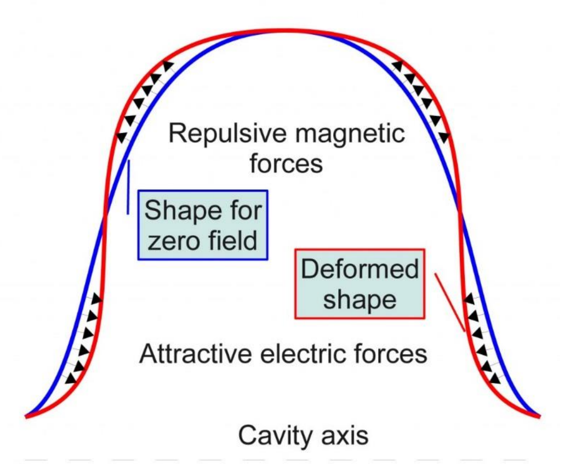

- Pressure variation in the surrounding He bath:

$\Delta f_{He} = df/dP \times \delta P$, δP~0.05-0.1 mbar at 2 K.

df/dP =30-130 Hz/mbar (ILC)

$$P_s = \frac{1}{4}(\mu|\vec{H}|^2 - \varepsilon_0|\vec{E}|^2)$$

$$\Delta f_0 = (f_0)_2 - (f_0)_1 = -K E_{acc}^2$$

- Internal and external vibration sources (microphonics);
- Radiation pressure from the RF field, Lorentz Force Detuning:

$\Delta f_{LFD} = k_L E^2$, k_L- Lorentz coefficient,

For typical elliptical cavities k_L~ -1 Hz/(MeV/m)^2.

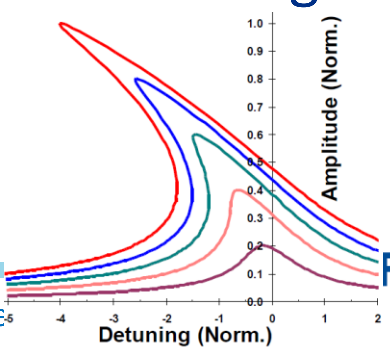

Microphonics:

- Detuned cavities require more RF power to maintain constant gradient
- Providing sufficient reserve increases both the capital cost of the RF plant and the operating cost of the machine
- **PEAK** detuning drives the RF costs
- Beam will be lost if RF reserve is insufficient to overcome PEAK detuning

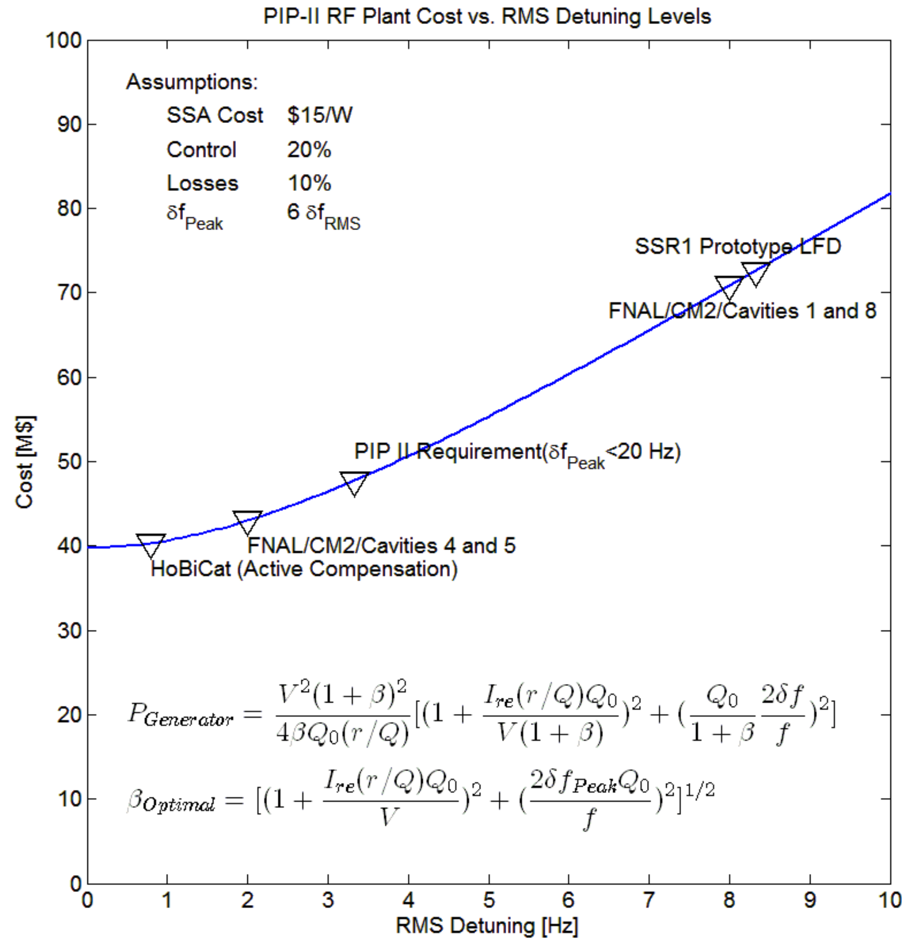

Microphonics Control Strategies

Microphonics can be mitigated by taking some combination of any or all of the following measures:

- **Providing sufficient reserve RF power to compensate for the expected peak detuning levels.**
- **Improving the regulation of the bath pressure to minimize the magnitude of cyclic variations and transients.**
- **Reducing the sensitivity of the cavity resonant frequency to variations in the helium bath pressure (df/dP).**
- **Minimizing the acoustic energy transmitted to the cavity by external vibration sources.**
- **Actively damping cavity vibrations using a fast mechanical or electromagnetic tuner driven by feedback from measurements of the cavity resonant frequency.**

The optimal combination of measures may differ for different cavity types.

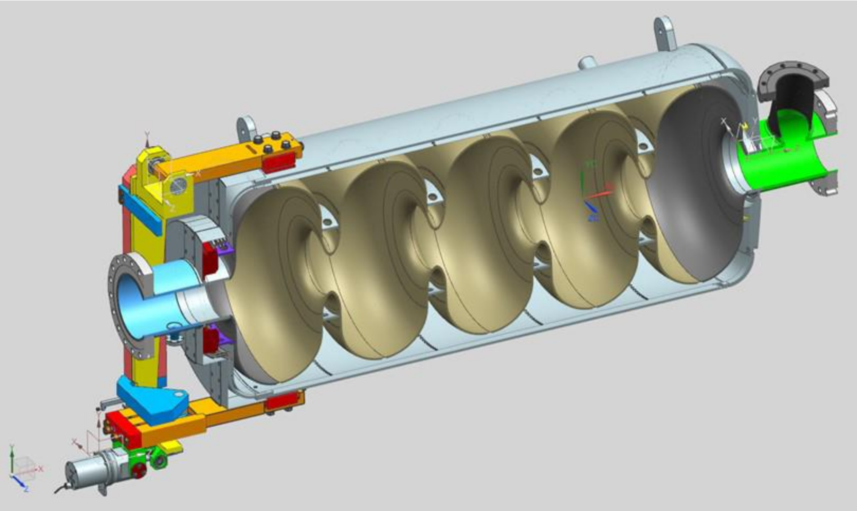

Thermal breakdown

- If there is a localized heating, the hot area will grow with field. At a certain field there is a thermal runaway and the field collapses (loss of superconductivity or quench).
- Thermal breakdown occurs when the heat generated at the hot spot is larger than that can be evacuated via Nb wall to the helium bath.

Temperature mapping

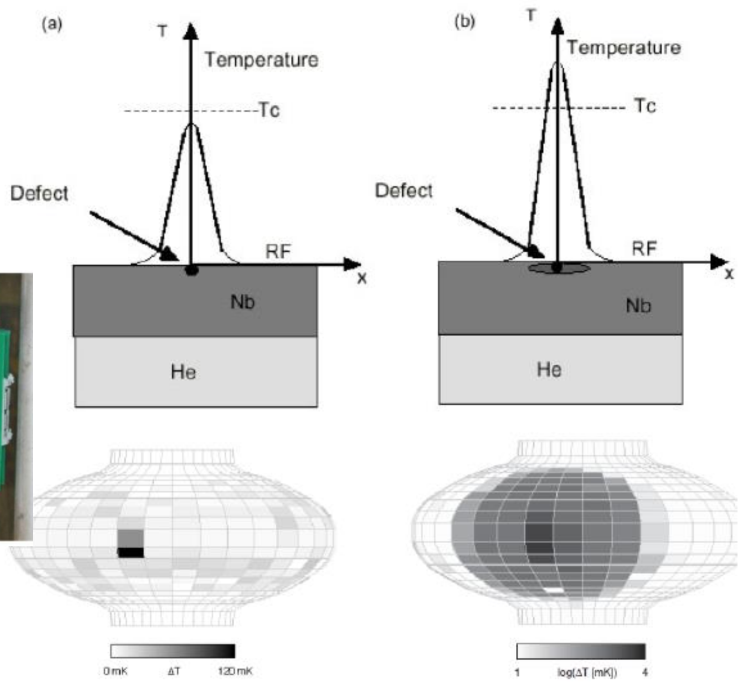

- Both the thermal conductivity and the surface resistivity of Nb are highly temperature dependent between 2 and 9 K.

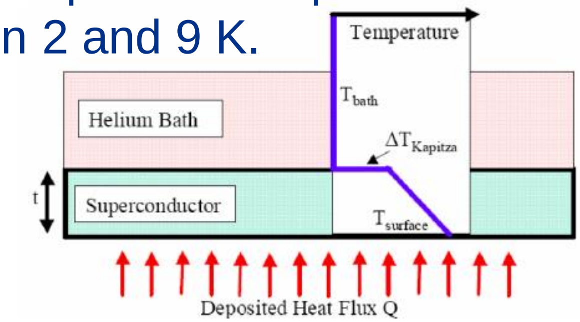

$$H_b^2 = \frac{T_0^2}{2 \cdot R_s(T_0) \cdot (\Delta \cdot T_c - T_0)} \cdot \left(\frac{k \cdot h}{k + h \cdot d} \right)$$

T_0 - He bath temperature,
T_c – critical temperature,
Δ – energy gap,
$h(T_0)$ – Kapitsa resistance,
$k(T_0)$ – thermal conductivity,

$$R_s(T) = R_0 \cdot \left[\frac{f\,(GHz)}{1.3} \right]^2 \cdot \left(\frac{T_c}{T} \right) \cdot e^{-\Delta \cdot \frac{T_c}{T}}$$

$R_0=10^{-5}\ [\Omega]$; $\Delta=1.8$; $T_c=9.2^oK$

Summary:

- SRF technology allows 1.e6 less surface losses than RT technology and consequently, much high acceleration gradient at high duty cycle or in CW regime;
- Losses at SRF are determined mainly by BCS resistance (inertia). flux trapping and intrinsic residual resistance;
- The acceleration gradient is limited mainly by thermal breakdown, field emission, etc., but not by breakdown.
- Modern cavity processing techniques (N-doping, etc.) allow very high Q_0.
- To achieve high Q_0 small residual magnetic field may be required, and therefore, good shielding and degaussing. The cryo-system should allow fast cooling for flux expulsion.
- Resonance discharge (multipacting) may be an issue; cavity processing is required; the cavity shape should be optimized.
- Field emission may limit the gradient; large-scale clean rooms are necessary among other means.